REPORT ON THE COOPERATIVE MINERAL
EXPLORATION IN THE KERIO VALLEY
DEVELOPMENT AUTHORITY AREA
REPUBLIC OF KENYA

PHASE II

MARCH 1986

METAL MINING AGENCY OF JAPAN
JAPAN INTERNATIONAL COOPERATION AGENCY

REPORT ON THE COOPERATIVE MINERAL EXPLORATION IN THE KERIO VALLEY DEVELOPMENT AUTHORITY AREA REPUBLIC OF KENYA

PHASE Ⅲ

MARCH 1986

JAPAN INTERNATIONAL COOPERATION AGENCY

METAL MINING AGENCY OF JAPAN

PREFACE

At the request of the Government of the Republic of Kenya, the Japanese Government planned and carried out a geological survey concerning mineral exploration to examine the possibility of the existence of mineral resources in the Kerio Valley Development Authority Area located in the northwestern part of Kenya. The Japan International Cooperation Agency was entrusted with the execution of the general plan. The Japan International Cooperation Agency in turn entrusted the execution of this survey to the Metal Mining Agency of Japan since this survey was essentially a professional survey of geology and mineral resources.
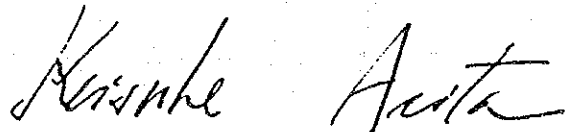
The Metal Mining Agency of Japan organized a survey team consisting of three members in 1985, the third year of the survey project, and despatched the team to Kenya during the period from July 28 to September 15, 1985.

The on-site survey was completed as scheduled with the cooperation of the Kenya Government, particularly the Kerio Valley Development Authority and Mines and Geological Department of the Ministry of Environment and Natural Resources.
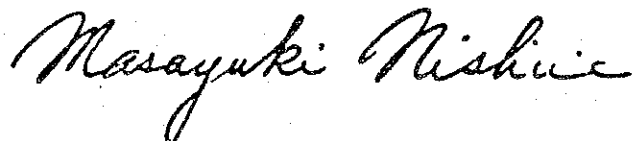
This report describes the survey results in the third year and will form part of the final report.

Lastly, we would like to express our heartfelt gratitude to the members concerned of the Government of the Republic of Kenya, the Ministry of Foreign Affairs of Japan and the Embassy of Japan in Kenya, and to all those who extended their kind cooperation to us in executing the above-mentioned survey.
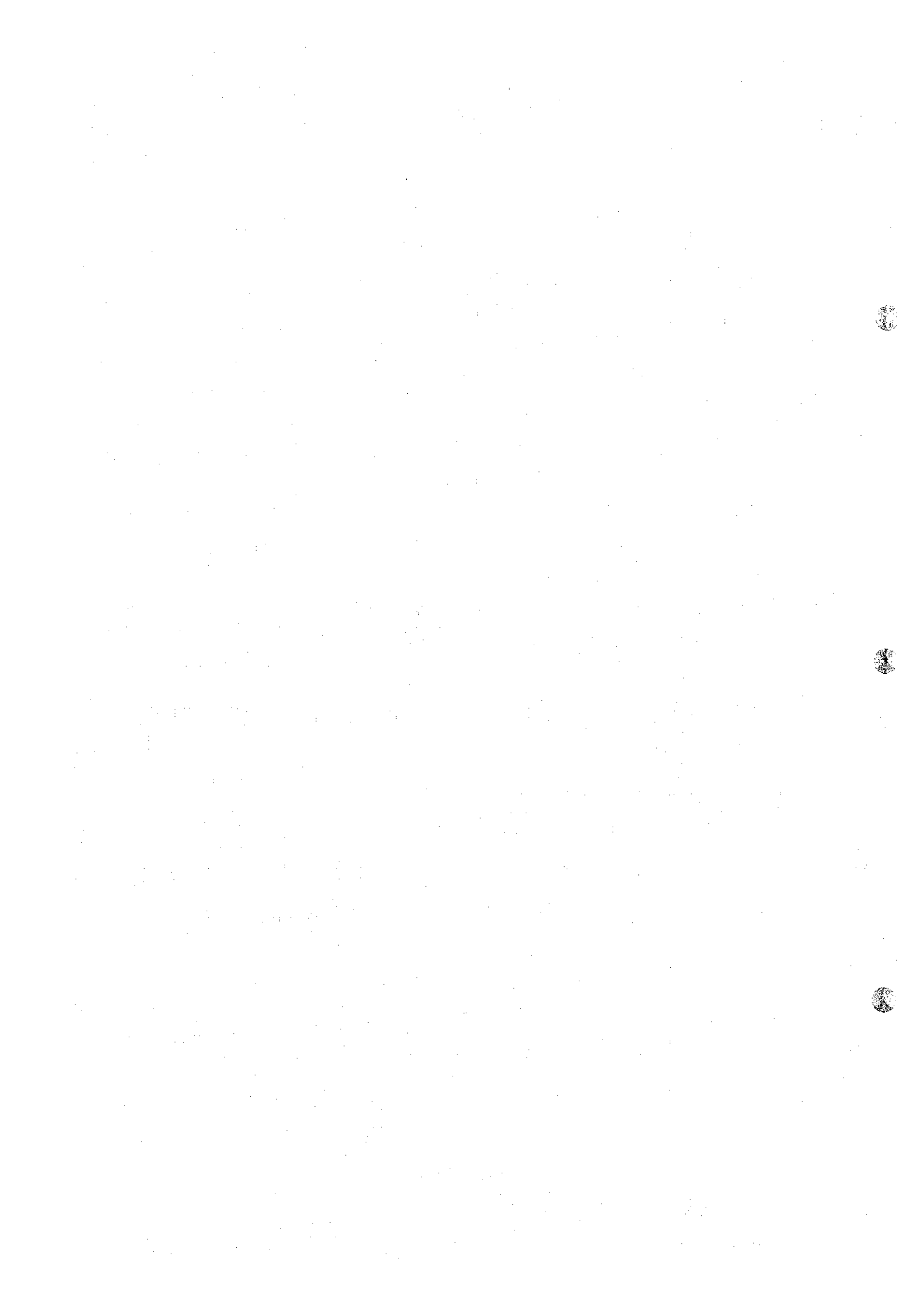
December, 1985

Keisuke Arita
President,
Japan International Cooperation Agency
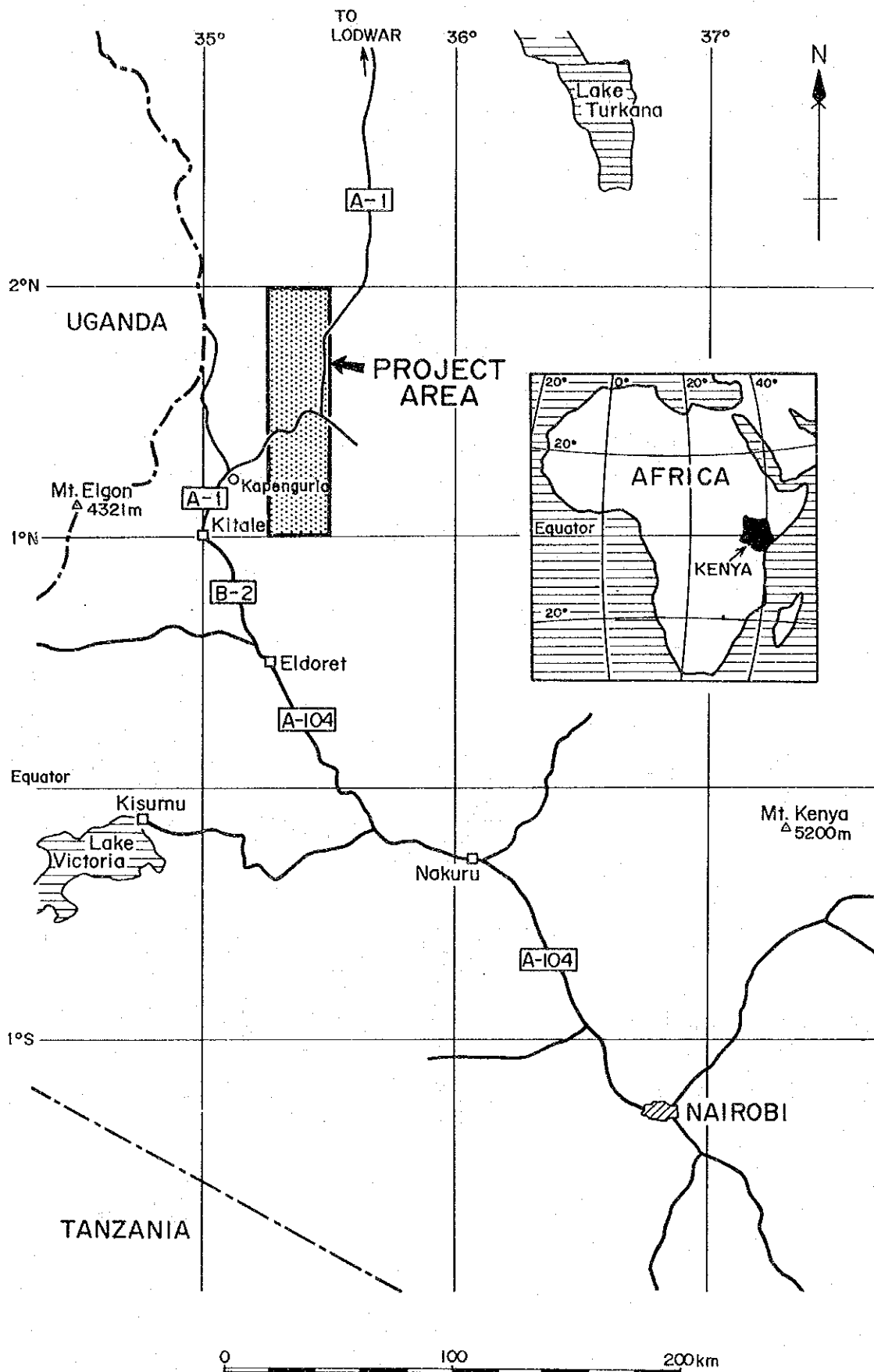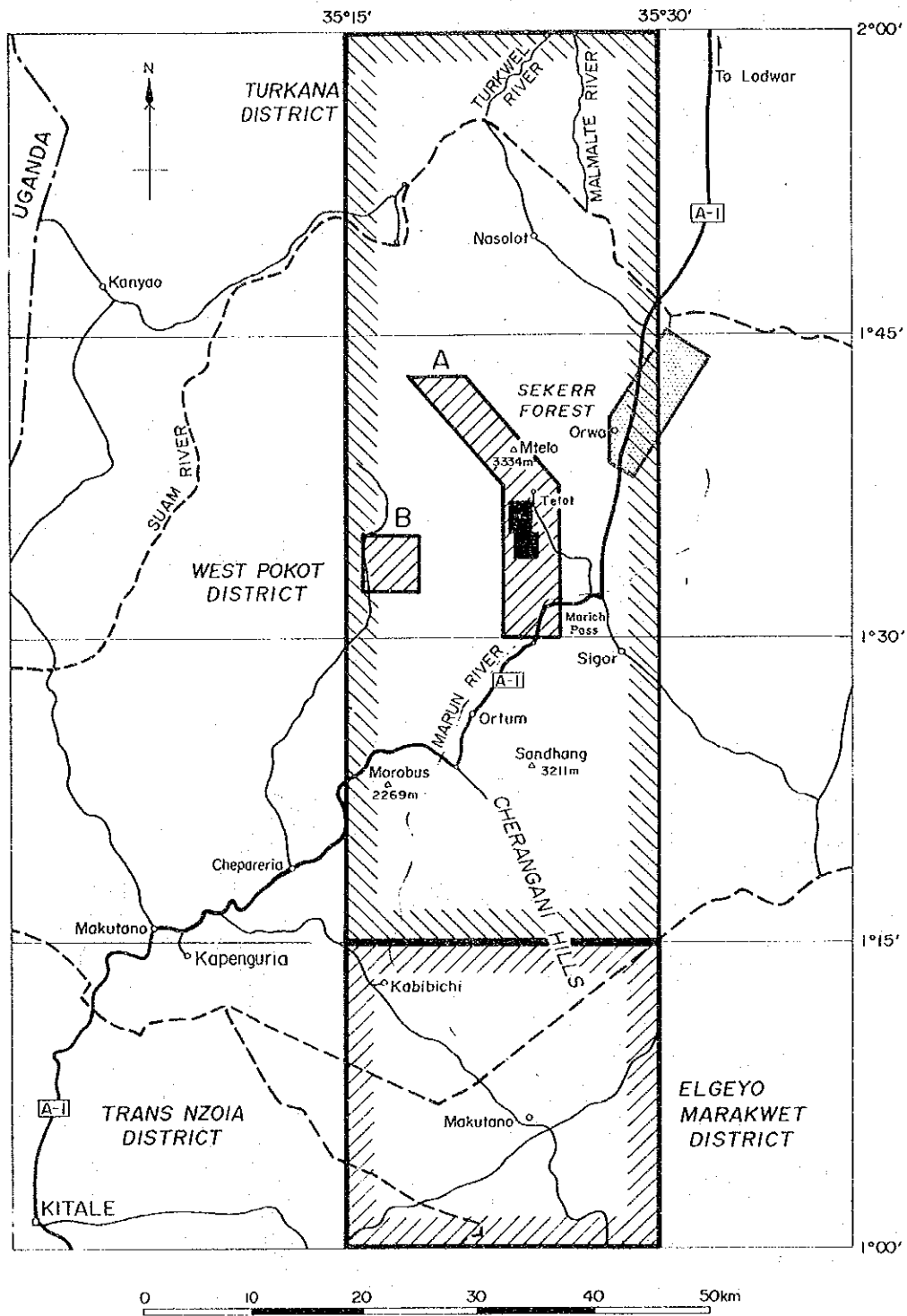
Masayuki Nishiie
President,
Metal Mining Agency of Japan

Fig. 1   Location Map of the Project Area

|	Phase I	Regional Survey Area
	Phase I	Semi-detailed Survey Area (A, B)
	Phase II	Regional Survey Area
	Phase II	Detailed Survey Area
	Phase III	Geophysical Survey Area

Fig. 2 Location Map of Phase Ⅲ Survey Area
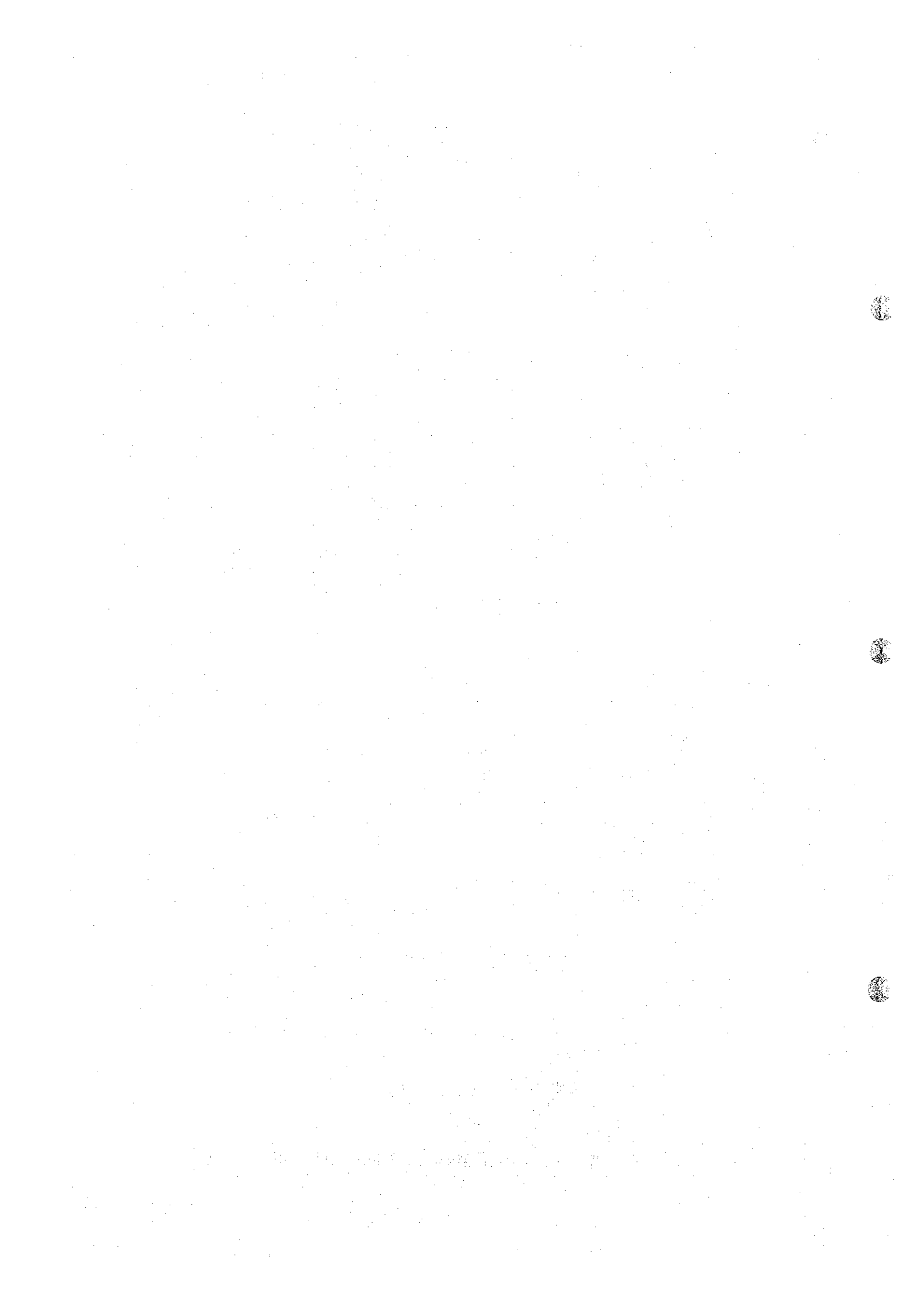
ABSTRACT

The cooperative mineral exploration project in the Kerio Valley Development Authority Area in the Republic of Kenya was conducted for three years from 1983 to 1985.

The purpose of the survey is to extract promising areas for occurrence of ore deposits in the survey area by comprehensively investigating the relationship between the geologic structure and mineralization as well as geochemical and geophysical characteristics in the area.

The area of geophysical survey is situated in the northeastern part of the regional survey area in the Phase I at the western end of the Eastern Rift Valley. The aeromagnetic survey had been conducted by the Kenya Government in the survey area, and strong magnetic anomaly was detected leading to an expectation that ultrabasic rock with strong magnetism might be distributed.

The survey was carried out for the purpose of clarifying the physical features of the ultrabasic rocks thought to be present by ground gravity survey and ground magnetic survey, and to investigate the possibility of occurrence of chromite ore deposit.

Geology of the area is composed of gneissose granite of the basement distributed at the western end of the area forming a zone and Quaternary alluvial formation is extensively distributed over most part of the area.

Northeastern trend of the geologic structure is conspicuously based on the distribution of gravitational anomalies and the fault structure steeply dipping southeastward is inferred on the western side of the area. This might indicate the fault at the western end of the Rift Valley. A boat-shaped basin structure with an increasing depth towards the southwest is assumed at the central part of the survey area. The base of the basin is estimated to be at about two hundred and fifty meters below the surface.

According to the ground magnetic survey, the rock masses detected by the aeromagnetic survey seem to form two series of magnetic anomalies in the northern part and a series in the southern part. It is highly possible that the magnetic rock mass in the northern part would be ultrabasic rock including serpentinite from the result of measuring of magnetic susceptibility, and it is judged that thinly extended peripheral parts of the funnel-shaped rock body might be caught as two series of strongly magnetic anomalies.

The peripheral part on the eastern side is 100 to 500 meters wide and six kilometers long, while the one on the western side is 200 to 400 meters wide and two kilometers long, being located at 50 to 200 meters below the surface. The central part seems to have the width of about one kilometer and to occur at a depth deeper than 250 meters from the surface.

The magnetic rock mass in the southern part is small in scale and it is assumed that the depth is greater or the rock has a low magnetic susceptibility.

If the rock mass in the northern part is serpentinite, occurrence of chromite deposit could be expected.

However, taking into consideration the scale of the rock mass and the size and the grade of the known ore deposit occurring in the Telot serpentinite mass, it is likely that the deposit comprises small podiform chromite bodies and exploration work to find out sufficient ore reserves to warrant economic operation would be pretty difficult. Moreover, taking account that the rock mass lies beneath the soft and thick alluvial formation and at deeper part, and taking the fact that the Weiwei River with plenty water flows at the central part of the mass the exploitation of the deposit would be pretty high in cost.

CONTENTS

LIST OF ILLUSTRATIONS

LIST OF TABLES

LIST OF PLATES

CHAPTER 1   INTRODUCTION

1-1   Introduction

1-1-1   Purpose of Survey

The cooperative mineral exploration project in the Kerio Valley Development Authority Area in the Republic of Kenya was intended to make clear the geologic classification of the area to extract promising areas for mineral resources.

The survey area of the third year of the project, is an area in which strong magnetic anomalies had been detected by the aeromagnetic survey and because of the distribution of the Telot serpentinite mass in which chromite ore deposit is emplaced at about ten kilometers to the southeast of the survey area, occurrence of chromite deposit is expected to be found in the area.

The important subject of the survey is to make clear the possibility of emplacement of chromite and nickel deposits by studying the distribution and physical properties of ultrabasic rocks by conducting gravity and magnetic prospecting survey.

1-1-2   Outline of Survey

Table 1-1 shows the outline of survey and Table 1-2 shows the amount of samples used for laboratory test.

The surveyed area is situated in the northern part of the regional survey area of the Phase I and to the northeast of the semi-detailed survey area A covering an area of 60 square kilometers.

Geophysical survey was carried out by three Japanese exports and five Kenyans. The latter include two geologists, two geophysicist and one survey engineer. They cleared and measured survey lines for 210 kilometers in total, conducted levelling and gravity measurement at 1,100 stations and carried out magnetic survey at 2,155 stations. The position of survey lines and stations were designed by use of topographic map of 1:10,000 scale produced from the aerial photograph.

La Coste and Romberg G-206 type gravimeter was used for gravity prospecting and Scintrex MP-2 type proton magnetometer was used for magnetic prospecting.

Table 1—1   Outline of Geophysical Survey

Method	Outline of Works		
Gravity Survey	Area covered	:	60 km²
	Length of surveyed line	:	210 km
	Station	:	1100 points
	Station interval	:	200 m
	Leveling	:	1100 points
Magnetic Survey	Area covered	:	60 km²
	Length of surveyed line	:	210 km
	Station	:	2155 points
	Station interval	:	100 m

Table 1—2   Laboratory Works Carried Out

Item	Amounts
Magnetic susceptibility	50
Density	50

1-1-3   Organization of Survey Team

The members engaged in planning, negotiation and field survey are as follows:

(1)   Planning and Negotiation in Kenya

Japanese Counterparts

Toshio Sakasegawa	Metal Mining Agency of Japan (MMAJ)
Yasuhisa Yamamoto	do.
Yoshiyuki Kita	do.
Yosuke Suzuki	MMAJ, Representative in Nairobi
Osamu Nakano	Japanese Embassy to Kenya
Noboru Akahoshi	Japan International Cooperation Agency (JICA)
Akira Takahashi	JICA, Representative in Nairobi
Norio Shimomura	do.
Mitsuru Suemori	do.

Kenyan Counterparts

S. K. Tubei	Kerio Valley Development Authority (KVDA)
A. M. Ngumi	do.
C. Y. O. Owayo	Mines and Geological Department (MGD)
F. G. Theuri	do.

(2)   Survey Team

Japanese Counterparts

Leader	Haruo Watanabe	Metal Mining Agency of Japan (MMAJ)
Member	Motoharu Takagi	do.
do.	Seiji Tsuchida	do.

Kenyan Counterparts

Leader	A.M. Ngumi	Kerio Valley Development Authority (KVDA)
Member	M.C. Lilako	do.
do.	J.J. Maneno	Mines and Geological Department (MGD)
do.	W. Muthigani	do.
do.	G.M. Kavuthi	do.

1-2　Outline of the Survey Area

1-2-1　Location and Communication

The project area is situated in the Rift Valley Province in the northwestern part of Kenya, and strides over the four district of West Pokot and Turkana, and partly over Trans Nzoio and Elgyo Marakwet, showing a rectangular form of about 3,070 square kilometers in area bounded by N1°00′-2°00′ latitude and E35°15′-35°30′ longitude. The area is within the domain of the Kerio Valley Development Authority (KVDA). The domain of KVDA includes the whole drainages of the rivers flowing into the Lake Turkana, and it was named after the Kerio Valley, which is a large river running northward at the central part of the basin. The domain also includes the Rift Valley in Kenya on the northern side of Equator.

The area in which geophysical survey was conducted is situated in the northeastern part of the project area and has an extent of 60 square kilometers centering on N1°40′ latitude and E35°30′ longitude.

The National Highway A-1 passes through the area of geophysical survey, which is situated at a distance of about thirty kilometers from Ortum, the center of the Kerio Valley Project area, is about five hundred kilometers from Nairobi, the capital city of Kenya.

1-2-2　Physiographical Features

The survey area is on the ighland composed of the Precambrian basement, and the topography of the area is greatly influenced by the formation of the Rift Valley by crustal movement after Oligocene and volcanic activity.

The Rift Valley runs through the eastern part of Africa divering into two zones of the East and the West in East Africa, and the East Rift Valley runs northward through the western part of Kenya.

The area in which the geophysical survey was carried out is located at the western end of the East Rift Valley and forms a flat land of semi-desert to bushland type underlain by the Quaternary alluvial formation, 700 to 800 meters above sea level, bordered by the Rift Valley fault.

In the northern part of the survey area, the Wei-Wei River of Lake Turkana system flows northward into the Lake Turkana.

The Orwa creek and Mahany creek which dry up in dry season flow eastward from the western mountains forming tributaries of Wei-Wei River.

1-2-3　Climate and Vegetation

The survey area is composed of bushland, and the climate shows equator-type annual varia-

tion with rainy and dry seasons each coming twice a year. It is divided into warm dry season from December to March, heavy rainy season from March to June, cool dry season from June to September and light rainy season from September to November. The annual precipitation, however, varies greatly with years, being often damaged by drought.

The climate of the area is semiarid, where the temperature rises more than 35°C in the day time and goes down 10°C at night. The annual precipitation is 300 to 800 millimeters.

The vegetation of the area is characterized by thorny trees and cactuses forming bush. In the survey area, maize and sugar cane are cultivated on a small scale along the creeks such as Wei-Wei and Orwa, and livestock such as cattle and goat is pastured.
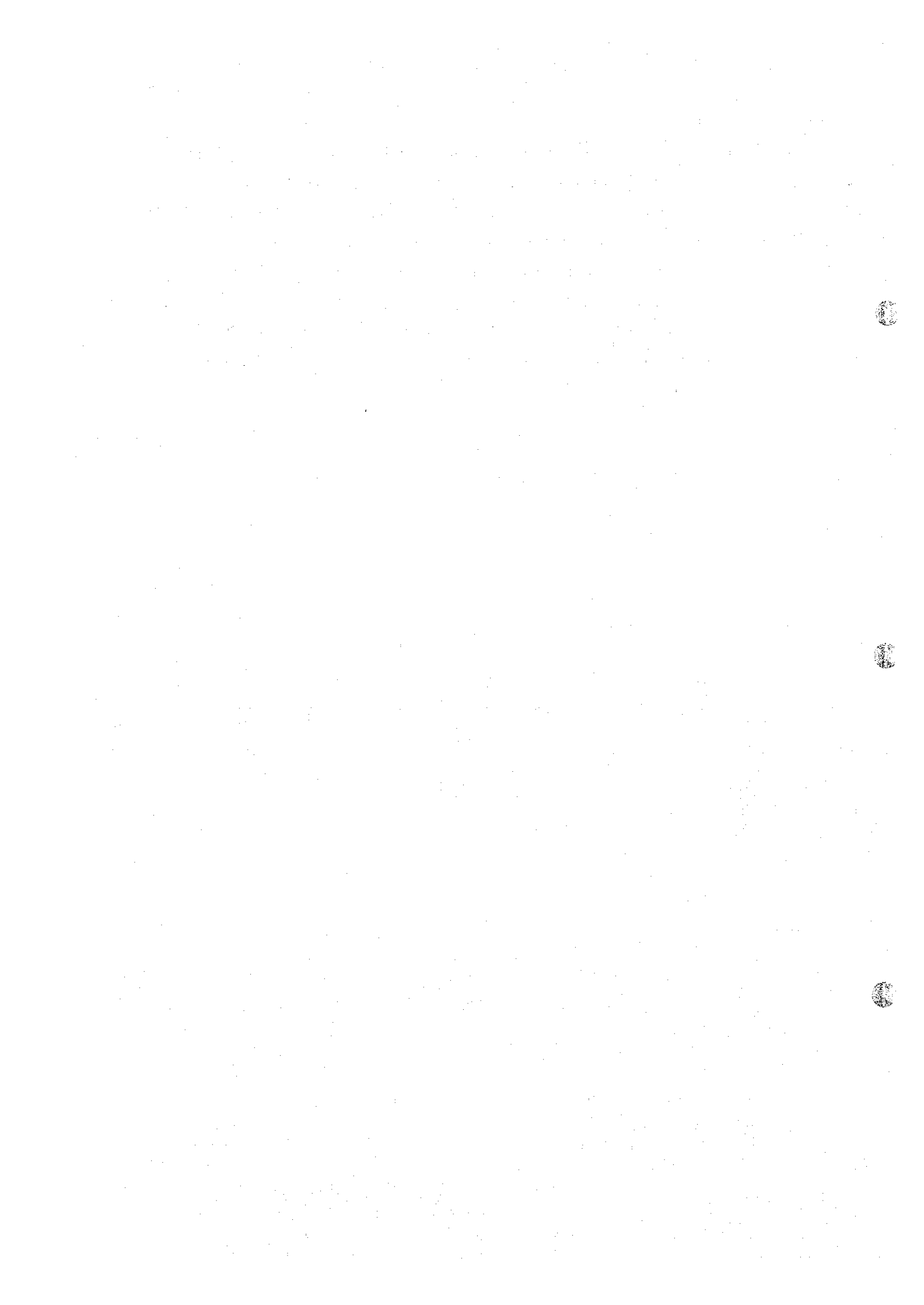
CHAPTER 2   RESULTS OF SURVEY

2-1   Setting of Survey Line

The survey area is located at the western end of the East Rift Valley of the African Rift Valley. Geology in the vicinity of the area consists of the Precambrian Mozambique metamorphic rocks belonging to amphibolite facies and the intrusive rocks intruding the former, showing a notable north-south trending structural pattern.

Although geology of the area is considered to be composed of metamorphic rocks and intrusive rocks ranging from granite to ultrabasic rocks, which is called the Mozambique belt rocks of Precambrian age, setting aside the northwestern part of the survey area where the basement rocks are well exposed, the rocks are hardly exposed in the flat area distributed by the Quaternary sediments occupying the most part of the area, where the form of distribution of basement rocks and intrusive rocks remains almost unknown.

However, because the geologic structure in the vicinity of the survey area is basically controlled by synclines trending north-northwesterly and because it is characterized by a number of overturned folds of the same trend and the faults of northerly to north-northwesterly trends, 56 survey lines each four kilometers long were set at right angles to the above structures in the direction of N62°48′W to S62°48′E with a spacing of 250 meters.

The observation stations were located at an interval of 100 meters, and the gravity prospecting was planned to be carried out at 1,100 stations with an interval of 200 meters, whereas magnetic prospecting was planned to be carried out at 2,155 stations at 100-meter intervals.

The survey was performed by three to five parties consisting of eight persons per party using pocket compass and 100-meter measuring tape.

The arrangement of survey lines and the observation stations are shown on Plate 1 and Fig. 2-1.
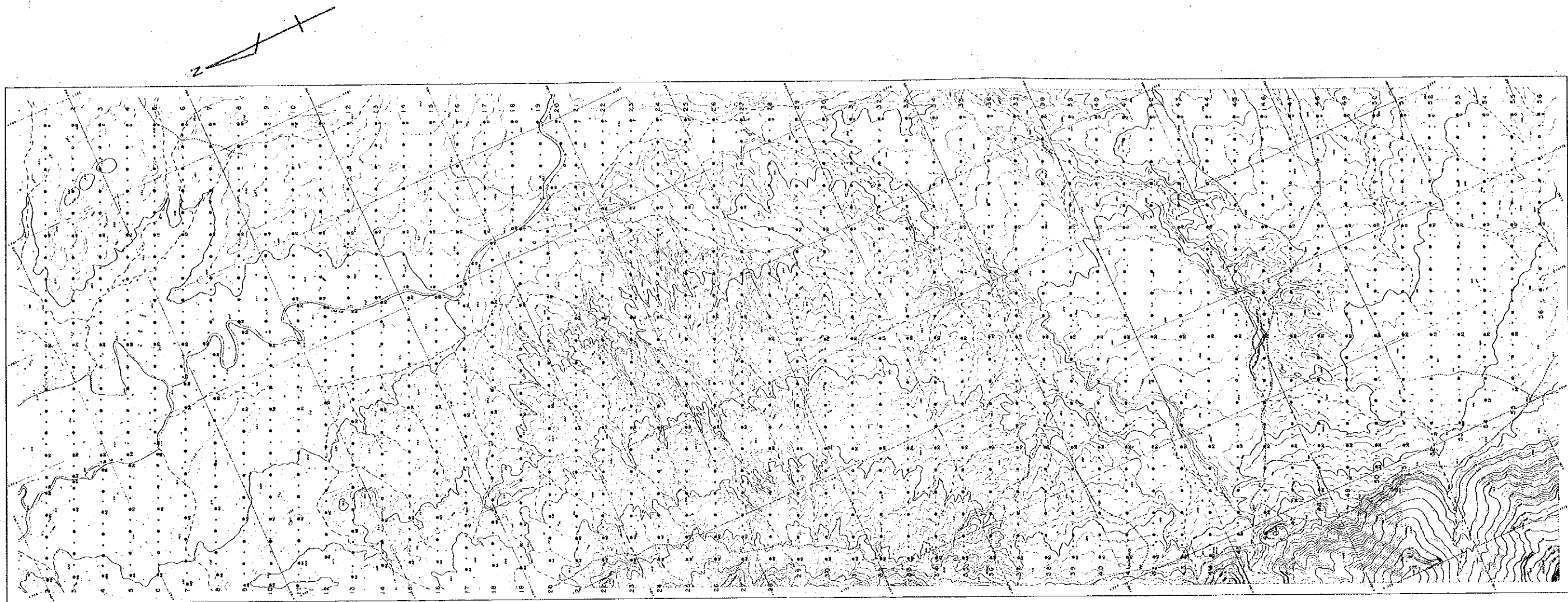
Fig. 2-1 Location Map of Magnetic and Gravity Survey Lines

LEGEND

Magnetic Observation Point and its Number
Magnetic and Gravity Observation Point and its Number

2-2   Gravity Prospecting

Gravity prospecting was conducted for the extent of 60 square kilometers in the Kerio Valley Project area for the purpose of clarifying the structure of the basement.

2-2-1   Method of Prospecting

1.   Survey Planning

Plate 1 and Fig. 2-1 show the arrangment of the survey lines and observation stations. Although the planned stations were to be 1,100 points, actual observation was performed at 1,118 stations, and the altitude of all these stations were measured by levelling. The survey area was about sixty square kilometers and the standard station interval was 200 meters, and the stations were located along surveyed and cleared lines.

2.   Gravimeter

La Coste and Romberg G type gravimeter was used. The specifications are listed in the following.

No. of Production	G-206
Operating Range	0.0 ~ 7335.25
Accuracy of Reading	± 0.01 mgal

La Coste gravimeter has the worldwide range without necessity of resetting and the drift is as small as less than 0.5 mgal per month, showing an excellent accuracy. La Coste gravimeter has its own particular correction parameter. The range of correction values is variable with the elevation and latitude of the survey area. The values for conversion parameter of the G-206 gravimeter used for the measured values of this time are shown below.

Counter Reading	Value in mgal	Factor for Interval
1300	1361.31	1.04730
1400	1466.04	1.04742

3.   Gravity Standard

The gravity base point was set as Wakorr 9000 at Wakorr, the base camp of the survey.

The gravity value of the base point was established by comparative measurement with the gravity standard station located at the Survey of Kenya (at about four miles to the northeast of the center of Nairobi). This gravity value was measured by pendulum in 1958 for its absolute

value, and it was set to be 977,540.4 mgal. The gravity value of Wakorr 9000 was decided 977,657.338 mgal.

Table 2-1   Gravity Standard Values

	Nairobi (Survey of Kenya)	Wakorr 9000
Latitude	1°14'55"S	1°29'40"N
Longitude	36°51'24"E	35°24'25"E
Date of Observation	1985.7.3	1985.7.4
Time of Observation	12h 27 m	10h 03 m
Reading Value	1225.271	1337.079
Milligal Value	1283.046	1400.143
Earth Tide Correction (mgal)	0.139	−0.020
Instrument Correction (mgal)	0.000	0.000
Corrected Value (mgal)	1283.185	1400.123
Gravity Value (mgal)	977,540.4	977,657.338

4.   Levelling

Elevation was measured for all the gravity observation point by direct levelling. The level used was Auto level B-2 of Sokkisha, Japan No. 73432.

As the basement of levelling, the elevation of the top of a hill 893 meters above sea level, in the vicinity of No. 38 point along the survey line 18 obtained by the photo survey, was used because of lack of bench mark or triangulation point to indicate accurate elevation in the neighborhood.

2-2-2   Data Processing and Method of Analysis
1.   Data Processing
1)   Calculation of Gravity Value

Calculation of the gravity values is carried out in accordance with the flow chart shown in Fig. 2-2.

This process includes such calculation as "milligal conversion" to convert the counter of gravimeter to the unit of gravity (mgal), "tidal correction" to correct the diurnal variation, "instrument height correction" relating to the position of observation of gravimeter and "drift
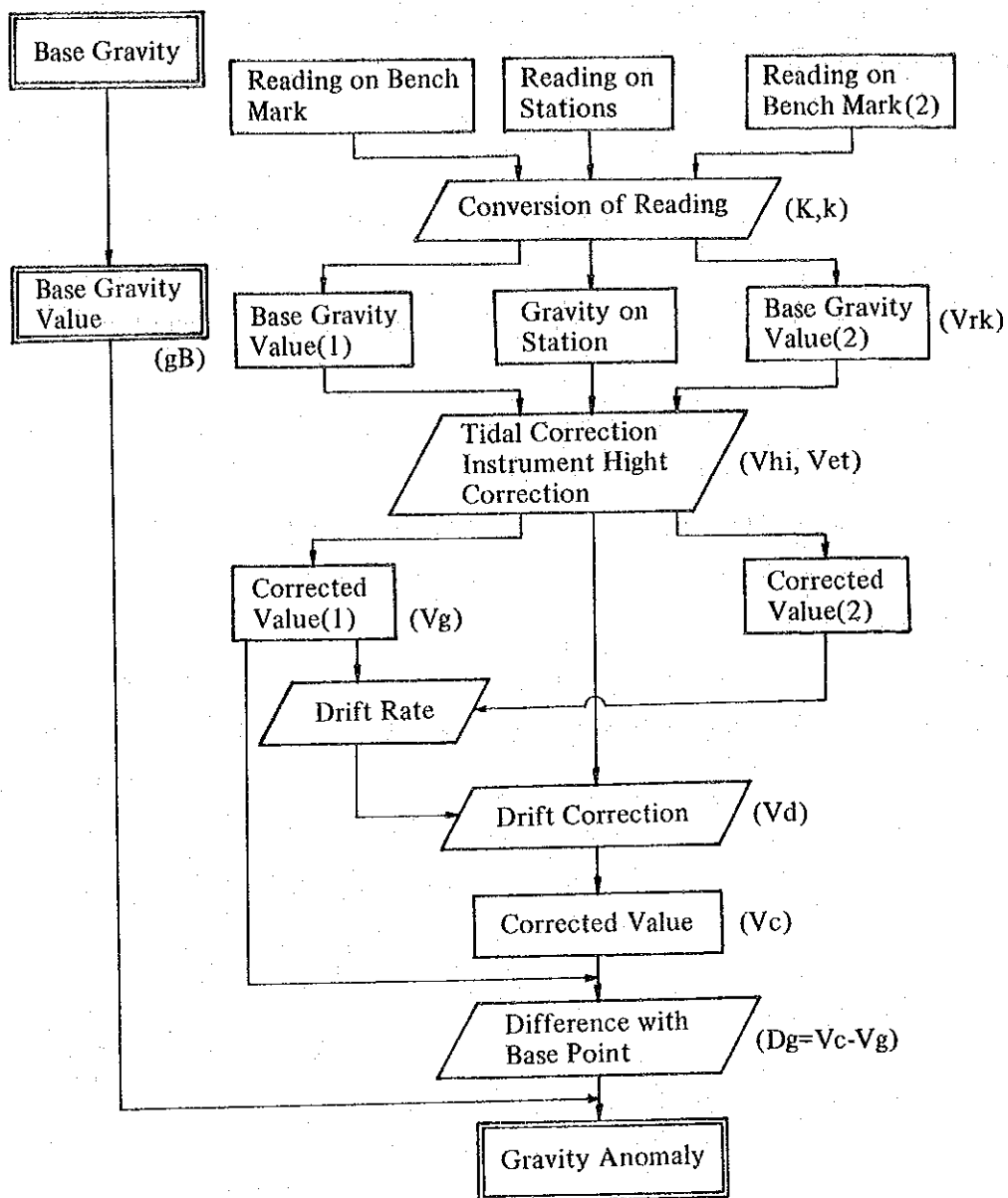
Fig. 2-2 Flow Chart of Gravity Data Processing

correction" to correct closure error at the standard point.

(1) Milligal Conversion

To obtain gravity in milligals from the reading of the counter and dial, a table of conversion is employed.

The table of gravimeter constant includes the constant (K: mgal) for each 100 units of the counter and scale constant (κ).

If the conversion factor is 3219.876, milligal conversion will be obtained by the following formula.

$$V_{rk} = K_{3200} + (3219.876 - 3200) \times \kappa_{3200}$$

where V_{rk} : Observed gravity value

          K_{3200} : Gravimeter constant indicated by 3200

          κ_{3200} : Scale constant (κ) indicated by conversion factor

(2) Tidal Correction

Tidal correction is the correction to remove the effect given to observation of gravity due to the attraction of the moon and the sun (tide generating force) and the deviation caused by the above. Tide generating force of the celestial bodies is calculated by the following formula.

$$U = \frac{3}{2} GM \frac{a}{r^3} [3 (\sin^2 \delta - \frac{1}{3}) \cdot (\sin^2 \varphi - \frac{1}{3}) + \sin 2\varphi \cdot \cos \theta \cdot \sin 2\delta + \cos^2 \delta \cdot \cos^2 \varphi \cdot \cos 2\theta]$$

where   U : Tidal force of celestial body

        G : Universal gravitation constant

        M : Mass of celestial body

        a : Distance from the center of the earth to the observation point

        r : Distance between celestial body and the earth

        φ : Latitude at observation point

        δ : Declination of the celestial body (angle from equator to south or north)

        θ : Angle of the celestial body (angle between meridian plane of the celestial body and that of observation point)

In connection with tide generating force, those caused by the moon and the sun are overwhelmingly great, so that only these two celestial bodies are taken into consideration in the ordinary gravity prospecting.

(3) Instrument Height Correction

This correction is used to adjust the instrument height from the station elevation surveyed by levelling, and generally it is obtained by conversion of counter value to that of the elevation

surveyed.

Mean vertical gradient of gravity 0.3086 mgal/m on the ground surface (strictly a spheroid) is used for correction, and it was done by the following formula.

$$V_{hi} = 0.3086 \ hi$$

Where V_{hi} : Instrument height correction (mgal)

hi   : The height from the station elevation to the top of gravimeter (m)

(4) Drift Correction

Drift is the displacement of counter values due to elongation of spring fixation system of gravimeter, which changes proportionally with time. While drift correction is to correct the displacement of counter value, the actual variation of counter value includes irregular displacement caused by mechanical shock and change of temperature and pressure of the atmosphere beside the one due to the drift, and drift correction includes all these in general. The correction is made by distribution of time allotment of closure error which is the difference of values after exerting tidal correction and instrument height correction to the counter value measured twice at the standard point.

(5) Calculation of Gravity Value

Corrected gravity value V_c is obtained from the following formula when each correction described in the above is exerting to the observed gravity value V_{rk}.

$$V_c = V_{rk} + V_{et} + V_{hi} + V_d$$

where V_c : Corrected gravity value

V_{rk} : Observed gravity value

V_{et} : Tidal correction value

V_{hi} : Instrument height correction value

V_d : Drift correction value

Drift correction is not required for the gravity value at the standard point, and corrected gravity value is obtained by exerting tidal correction and instrument height correction.

Gravity values at each survey point can be calculated by the following formula.

$$g = g_B + (V_c - V_g)$$

where   g   : Gravity value at survey point

g_B : Gravity value at standard point

V_g : Corrected value at standard point

2) Correction of Gravity

Correction of gravity is a series of calculation to obtain Bouguer anomaly which reflects subsurface structure by exerting various corrections to gravity value, and the calculation is made by separate corrections such as latitude, terrain, Bouguer and free air.

(1) Latitude Correction

Latitude correction was made by standard gravity. The standard gravity τ can be obtained from the following formula by using latitude φ of the survey point.

$$\tau = \frac{a\tau_E \cos^2 \varphi + b\tau_p \sin^2 \varphi}{\sqrt{a^2 \cos^2\varphi + b^2 \sin^2\varphi}}$$

where a : Radius of the spheroid at the equator (6378.14 km)

        b : Radius of the spheroid at the pole (6356.18 km)

       τ_E : Standard gravity at the equator (978.032 gal)

       τ_p : Standard gravity at the pole (983.218 gal)

The formula in the above is the one authorized by IUGG (International Union of Geodesy and Geophysics) as a formual to give the standard gravity of the earth in the Geodesy Standard System 1976.

For practical use in gravity prospecting, the standard gravity formula is used by expanding it in an approximate formula as in the following (practical formula of standard gravity).

$= 978031.85 \, (1 + 0.005278895 \sin^2\varphi + 0.000023462 \sin^4\varphi) \, (\text{mgal})$

(2) Terrain Correction

Terrain correction is to correct the influence given to gravimeter by topographic irregularity in the surrounding area of the survey point.

In the case of flat landforms, the amount of correction is zero, whereas steep topography might result in that the amount of correction would reach several tens milligals. The amount of correction always takes positive value for either correction of the mountainous part higher than the survey point or that of the part of valley lower than the survey point.

The topographic correction was calculated by dividing topography of the area around a station into three compartments of topographic group according to the difference of distance from the survey point.

The range and size of these topography are shown in Table 2—2.

(a) Terrain Correction of Far and Near Topography

The topographic correction of far and near areas was done by the use of disc divided into sections for topographic correction as shown in Fig. 2—3. The altitude of topography at the

Table 2-2 Range of Topographic Correction

Name of Topography	Range of Correction	Topographic Map Used for Correction
Far	0.4 – 10 km	1 : 50,000
Near	0.02 – 0.4 km	1 : 10,000
Neighbor	0.00 – 0.02 km	Sketch

center of the sections for correction was regarded as the mean altitude of each section to calculate the amount of correction of each section, and the total value of these was regarded as the amount of topographic correcion. The range of 400 meters to 10 kilometers was divided into 64 sections for the correction of far area and that of 20 meters to 400 meters into 24 sections for the near area, and correction was made by the use of Hammer's method.

The calculation formula used is shown below.

$$\delta g_T = \frac{2\pi G \rho}{n} \left(R_2 - R_1 + \sqrt{R_1^2 + H^2} - \sqrt{R_2^2 + H^2} \right)$$

where
δg_T : Terrain correction value

G : Gravitation constant

ρ : Density

R_1 : Distance to the inside diameter of a concentric cylinder

R_2 : Distance to the outside diameter of a concentric cylinder

H : Difference of altitude between correction section and survey point

n : Number of equal parts within a correction section
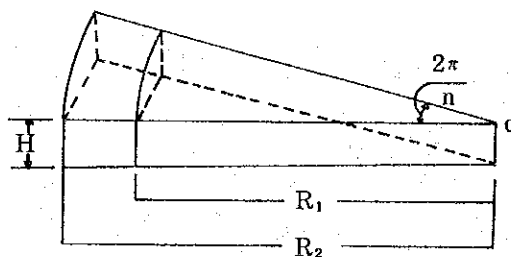
(b) Terrain Correction of Neighboring Topography

The correction of "neighbor" was made by expressing topographic irregularity within 20 meters from the survey point on a two-dimensional topogrpahic section from the survey point.

block number

R_4	:	0.4^{km}	
			8
R_5	:	1.0	
			8
R_6	:	2.0	
			12
R_7	:	3.3	
			12
R_8	:	5.0	
			12
R_9	:	7.0	
			12
R_{10}	:	10.0	

Far

block number

R_1	:	20^m	
			4
R_2	:	100	
			8
R_3	:	200	
			12
R_4	:	400	

Near
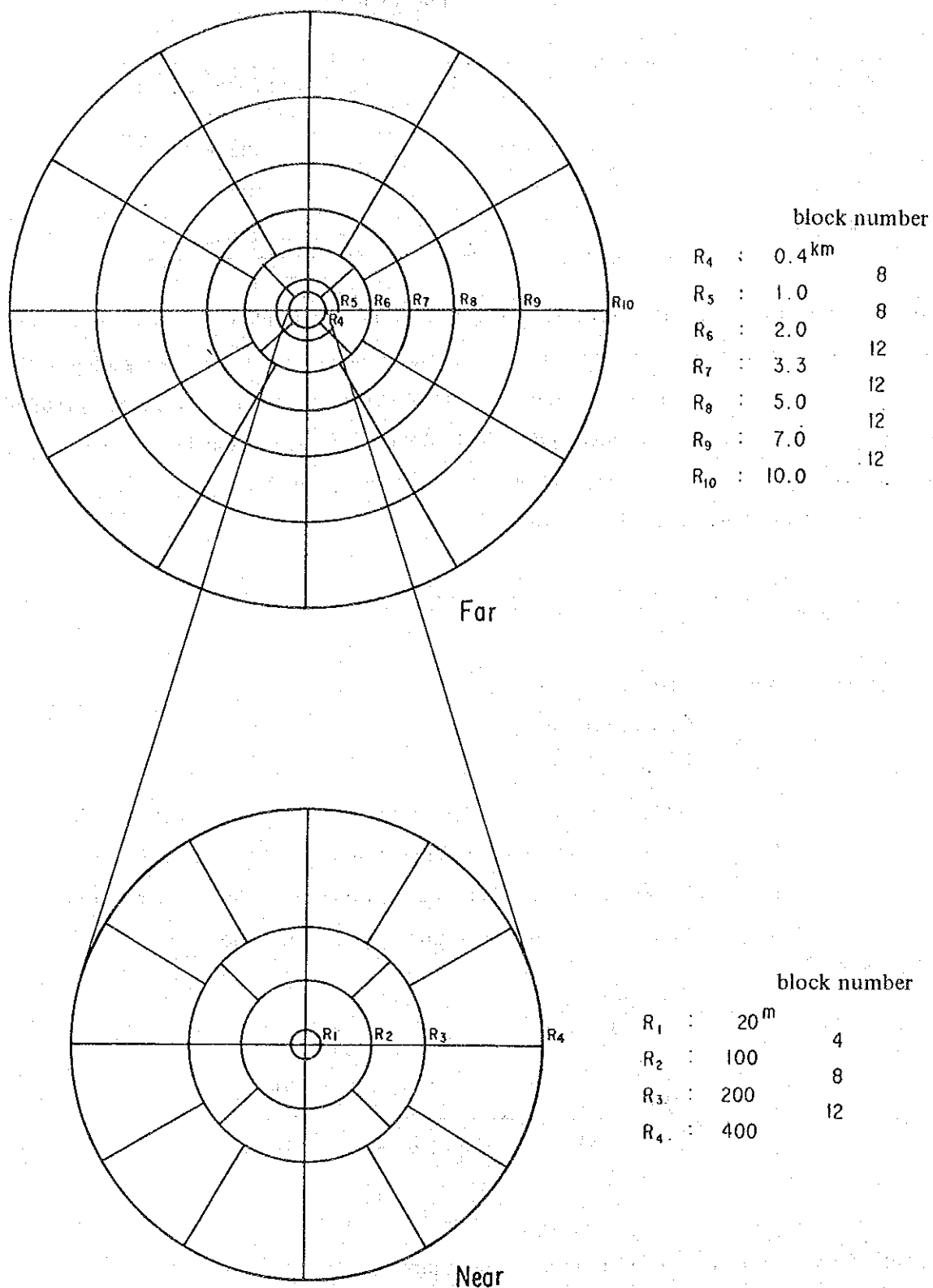
Fig. 2-3 Disc used for Terrain Correction

The formula for correction and conceptual figure are shown in the following.

$$\delta g_T = 2G\rho \int_D^R \left\{ \tanh^{-1}\sqrt{\frac{R^2 - X^2}{R^2 + H_0^2}} - \tanh^{-1}\sqrt{\frac{R^2 - X^2}{R^2 + (X\tan\beta + H - Ho - D\tan\beta)^2}} \right\} dX$$

where δg_T : Terrain correction value

G : Gravitation constant

ρ : Density

D : Distance from the survey point to the cliff

H : Height of cliff

β : Angle of inclination of cliff

R : Range of correction

Ho : Height of weight of gravimeter (0.15 m)
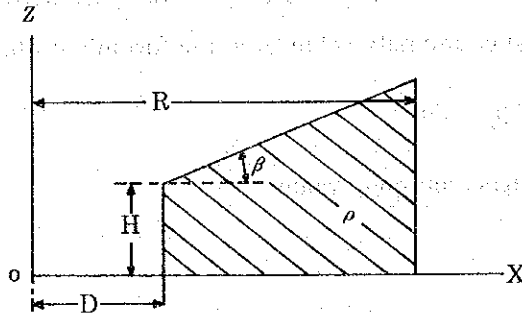
(3) Bouguer Correction

The gravity value observed at different height should differ for each other caused by the attraction of the material (rock mass) intervened between the different altitude, and Bouguer correction is one of the height correction to remove the influence of the material intervened between a certain standard plane and the plane parallel to the standard plane passing each survey point. Geoid plane is commonly used as the standard plane.

Correction was made by the following formula assuming that the part between geoid plane and that parallel to the standard plane passing the survey point is a infinite flat board.

$$\delta g_B = -2\pi G\rho H \doteqdot -0.0419\,\rho H$$

where δg_B : Bouguer correction value

G : Gravitation constant (6.670 x 10^{-3} cm^3/g sec^2)

ρ : Density of correction (g/cm^3)

H : Altitude of survey point (m)

ρ is Bouguer density, and mean density of rock intervened between the earth surface and

geoid plane is generally adopted.

(4) Free Air Correction

Free air correction is to correct the difference of gravity caused only by the difference of altitude, and the calculation was made by the following formula using the average vertical gradient 0.3086 mgal/m at the ground surface.

$$\delta g_F \doteqdot \frac{2\tau}{R} H \doteqdot 0.3086\ H$$

where δg_F : Free air correction value (mgal)

τ : Standard gravity (mgal)

R : Distance from survey point to the center of the earth (m)

H : Altitude of survey point

(5) Bouguer Anomaly

Exertion of latitude correction, terrain correction, Bouguer correction and free air correction results in obtaining Bouguer anomaly value from the formula in the following.

$$\Delta g_B = g - \tau + \delta g_T + \delta g_B + \delta g_F$$

where Δg_B : Bouguer anomaly value

2. Method of Analysis

The gravity anomaly observed on the surface is the overlap of gravity anomalies due to subsurface structure having various depth and various form. Therefore, it is required to express accurately and readily the subsurface structure to be aimed at, and to analyze. For this purpose, the anomaly is analyzed applying filtering to Bouguer anomaly map. In this survey, residual gravity value was calculated by running average method.

Next, two-dimensional quantitative analysis was made by two layered structure composed of basement formation and Quaternary alluvial mantle formation in order to make clear the basement structure of the survey area.

In case of analysis of these, the accuracy of analysis depends greatly upon how to assume the density of rocks and formations distributed in the survey area.

1) Assumption of Density

While it is necessary to assume the density to produce Bouguer anomaly map, it is very difficult to express the subsurface structure as the density structure, so that the assumption would have to be made from several data.

Table 2-3 Density and Susceptibility of Rock Samples

| Group	Sample No.	Rock Name	Location	Density (gr/cm³)			Susceptibility (x10⁻⁶ cgs-emu)	
				Dry	Wet	Average	emu/cm³	Average
Siliceous Dikes	1	Silicified brecciated rock	0/50	2.65	2.66	2.55 (2.57)	60.9	235.7
	2	"	23/32	2.52	2.53		232.2	
	3	"	9/42	2.49	2.52		414.0	
Basalts	4	Basalt	5/11	2.83	2.84	2.80 (2.82)	402.2	435.5
	5	"	3/13	2.81	2.82		682.3	
	6	"		2.80	2.82		774.0	
	7	"	3/10	2.81	2.83		386.3	
	8	"	2/13	2.81	2.83		598.5	
	9	"	2/7	2.80	2.82		231.0	
	10	"	2/9	2.76	2.79		198.6	
	11	"	4/4	2.78	2.80		211.2	
Gabbros	12	Gabbro	Wakorr	2.96	2.97	2.94 (2.95)	211.2	197.1
	13	"	"	2.91	2.92		183.0	
Serpentinites	14	Serpentinite	Telot	2.78	2.79	2.69 (2.71)	5,401.3	4,532.6
	15	"	"	2.69	2.70		4,816.4	
	16	"	"	2.58	2.59		3,122.1	
	17	Silicified serpentinite	"	2.61	2.63		4,175.4	
	18	Talc rock	"	2.81	2.83		5,147.6	
Chromite Ores	19	Chromite ore	"	3.85	3.87	3.84 (3.86)	259.9	382.8
	20	"	"	3.83	3.85		505.6	
Foliated granites	21	Granite	14/41	2.46	2.51	2.52 (2.54)	101.8	202.5
	22	"	10/44	2.54	2.56		221.0	
	23	"	Wakorr	2.59	2.60		310.0	
	24	"	?	2.52	2.55		54.6	
	25	"	22/40	2.55	2.57		144.1	
	26	"	22/41	2.49	2.52		159.4	
	27	"	?	2.51	2.55		722.1	
	28	"	52/34	2.59	2.60		167.2	
	29	"	23/36	2.56	2.58		47.6	
	30	"	23/35	2.49	2.52		157.2	
	31	"	24/39	2.52	2.55		113.9	
	32	"	53/32	2.54	2.57		24.1	
	33	"	21/40	2.50	2.54		74.0	
	34	"	52/30	2.56	2.58		144.1	
	35	"	48/38	2.57	2.59		170.8	
	36	"	12/34	2.44	2.47		301.3	
	37	Silicified granite	9/37	2.48	2.50		227.5	
	38	"	9/38	2.39	2.42		397.8	
	39	"	11/40	2.49	2.52		309.9	
Basic schists	40	Hornblend -chlorite schist	Telot	2.87	2.89	2.81 (2.84)	190.2	121.3
	41	Chlorite schist	"	2.72	2.75		62.5	
	42	"	"	2.84	2.87		111.2	
Siliceous schists	43	Muscovite-quartz schist	Turkwel Gorge	2.55	2.58	2.57 (2.60)	333.9	321.1
	44	"	"	2.56	2.59		402.7	
	45	Quartz schist	Telot	2.60	2.62		226.7	
Hornblend gneisses (Amphibolites)	46	Hornblend gneiss	Just NW to the Area	3.11	3.13	3.07 (3.08)	115.1	183.3
	47	"	"	3.19	3.20		256.6	
	48	"	26/42	3.06	3.06		269.5	
	49	"	Turkwel Gorge	3.12	3.14		223.3	
	50	"	Telot	2.86	2.89		52.1	
Biotite gneisses	51	Biotite gneiss		2.60	2.61	2.79 (2.81)	231.2	285.2
	52	"	20/41	3.01	3.03		261.3	
	53	"	Old Road (Orwa)	2.82	2.83		193.6	
	54	"	Turkwel Gorge	2.84	2.86		392.1	
	55	"	Orwa	2.69	2.70		347.7	
Average				2.69	2.71	2.70		683.9

( ) wet
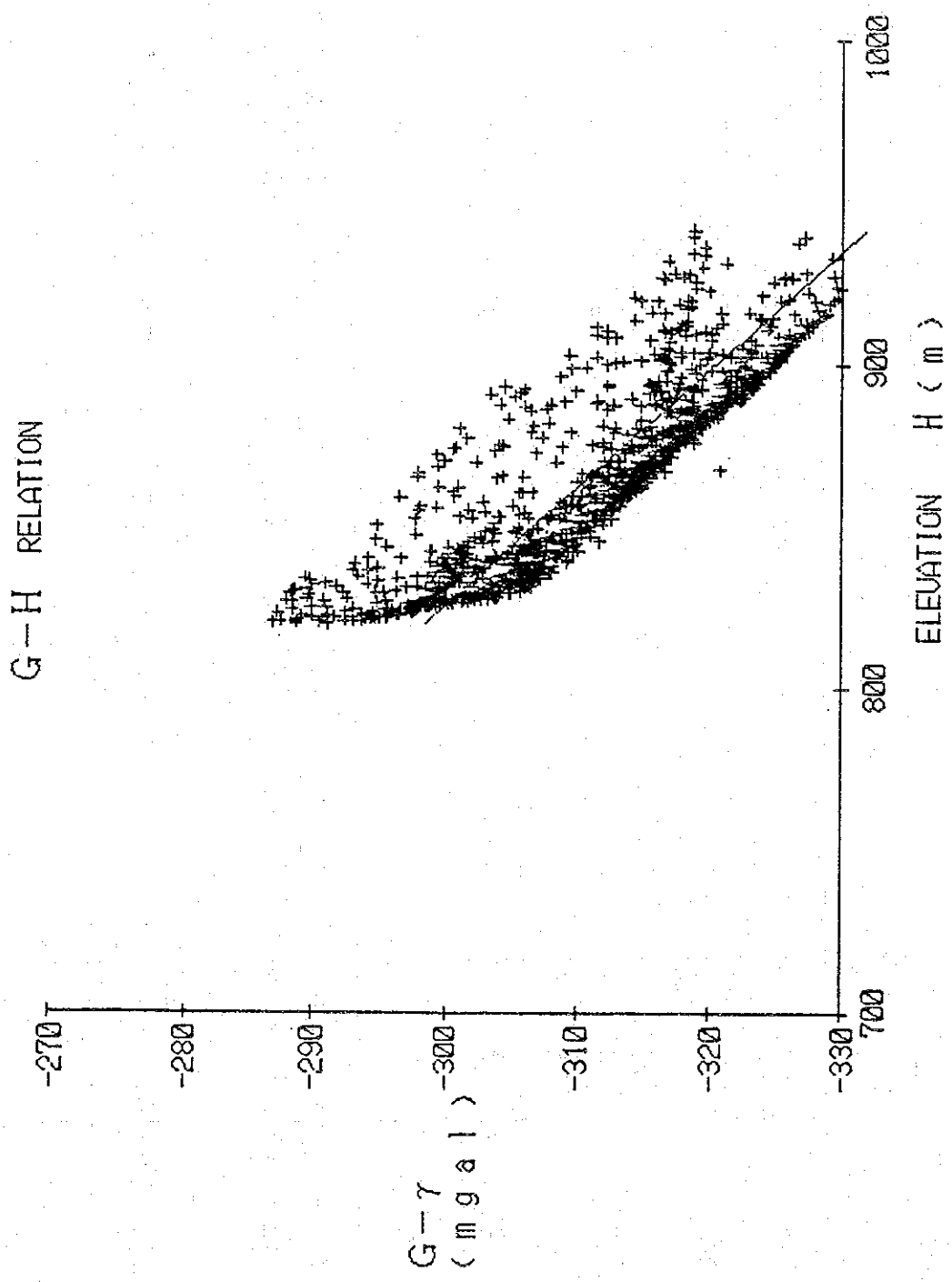
G—H RELATION

Fig. 2-4 G-H Correlation

(1) Measurement of Density of Rock Samples

In this survey, 55 rock samples were collected on the ground surface and their dry and wet density was measured. Table 2–3 shows the result of measurement of samples and average density for each rock.

The samples of serpentinite, chromite ore and a part of basement rocks were collected from the areas outside the survey area.

The Precambrian Mozambique metamorphic rocks constitute the basement of the survey area, which is intruded by the intrusive rocks. While the basement rocks are mainly composed of gneissose rocks and quartzite derived from pelitic to psammytic sedimentary rocks and basic volcanic rocks, the average density of these were 2.57 to 3.07 g/cm^3 in natural state. In terms of intrusive rocks, the density of gabbro was 2.94 g/cm^3 followed by 2.69 g/cm^3 of serpentinite, and granite showed relatively small value of 2.54 g/cm^3. Basalt showed relatively greater value of 2.80 g/cm^3. Chromite showed a great value of 3.84 g/cm^3.

The total average of all the rock samples except chromite ore was 2.70 g/cm^3.

It is difficult to assume the distribution of gravity anomaly from the average density of each rock as the geologic structure has not been made clear, because the density variation of basement rocks (2.57 − 3.07 g/cm^3) and that of intrusive rocks and volcanic rocks (2.52 − 2.94 g/cm^3) are almost in the same range. However, since the blanket formation over the basement rocks in the survey area consists of Quaternary alluvial formation and it is unconsolidated, it is presumed that the difference in density between the blanket and the basement rocks might be great. Accordingly, two layers of the basement rocks and the blanket formation can be assumed in general for the density structure of the survey area.

(2) G-H Correlation

Gravity value decreases with the altitude of survey point. The rate of decrement is nearly equal to the total of free air correction and Bouguer correction, 0.3086 − 0.0419ρ. Therefore, the average rock density ρ can be assumed from the gradient of the linear line formed by the plotted gravity data when the altitude of survey point is plotted on the axis of abscissas and latitude-corrected gravity on the axis of ordinates.

Fig. 2–4 (G-H Correlation) shows the relationship between the altitude of survey point and gravity.

In this survey, it seems to be difficult to assume the average density from the figure showing G-H correlation, because of very wide scattering of data on the figure due to small difference of elevation in the survey area which averages 100 meters.

(3) Determination of Corrected Density

Although the average density of the rock samples is 2.70 g/cm^3, occurrence of cracks in the rock and presence of the Quaternary formation have to be taken into consideration. Since it is proved that the gravity contour of ρ = 2.60 g/cm^3 shows good correlation with the geology of the area, the gravity contour of ρ = 2.60 g/cm^3 was used for the analysis.

2) **Filter Analysis**

While gravity distribution expressed on the Bouguer anomaly map is caused by the anomaly of subsurface density distribution, it is the sum of anomalies of density distribution of rocks which is different in depth and scale.

Filter analysis is to extract the anomalies which reflect best the subsurface structure to be aimed at.

In this survey, the figure of standard structure was produced by the use of Seya's method.

Residual gravity is obtained by the following formula.

$$\Delta G = \frac{1}{21} [4G_0 + 8\overline{G}\,(s) - 6\overline{G}\,(2s) - 6\overline{G}\,(3s)]$$

where ΔG : Residual gravity

    G_0 : Gravity of the station

    $G(ns)$: The average of four gravity value on the circle such that the radius is ns

    s : Sampling interval (200 m)

3) **Two-dimensional Analysis**

Geological structure causing the gravitational anomaly is assumed to be as follows;

(i)   Aggregate of polygonal structures with different density.

(ii) Stratified structure of which variation of subsurface density is the function of depth.

(iii) Two layered structure with the sediments of homogeneous density and the basement.

It is common to analyze the various residual gravity with various combination of those solution mentioned in the above in accordance with the geology of the survey area.

Among those solutions, the result of analysis on the area considered to be of the stratified structure is often utilized because it is able to give a relatively good explanation of the geologic structure.

Various manuals have been designed for the method of analysis in such case.

For the analysis in this survey, Talwani's method, which had been utilized in general, was

adopted.

Talwani's Method:

In two-dimensional section analysis, Bouguer values calculated from assumed density model are compared with the observed Bouguer values. The density structure model is to be obtained by modifying until the calculated Bouguer values fit well with the observed values by trial and error.

The calculation was made by the use of Talwani's standard formula shown in the following.

$$\Delta g = 2G \Delta \rho \Sigma Z_i$$

$$Z_i = \frac{(X_{i+1} - X_i) \cdot \{Z_i (X - X_{i+1}) - Z_{i+1} (X - X_i)\}}{(X_{i+1} - X_i)^2 + (Z_{i+1} - Z_i)^2}$$

$$\times \left\{ \tan^{-1} \frac{Z_i}{X_i - X} - \tan^{-1} \frac{Z_i + 1}{X_{i+1} - X} + \frac{1}{2} \cdot \frac{Z_{i+1} - Z_i}{X_{i+1} - X_i} \cdot \log \frac{(X_{i+1} - X)^2 + Z_{i+2}^2}{(X_i - X)^2 + Z_i^2} \right\}$$

Provided that when a side of the polygon is vertical ($X_i = X_{i+1}$)

$$Z_i = \frac{X_i - X}{2} \cdot \log \frac{(X_i - X)^2 + Z_{i+2}^2}{(X_i X)^2 + Z_i^2}$$
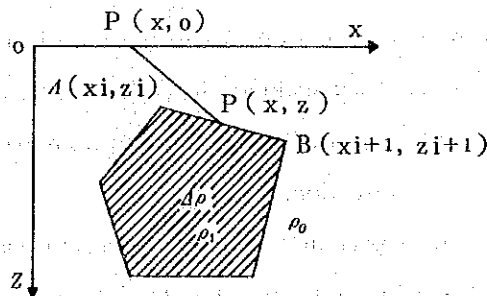
and, when a side of the polygon is horizontal ($Z_i = Z_{i+1}$)

$$Z_i = -Z_i \left(\tan^{-1} \frac{Z_i}{X_i - X} - \tan^{-1} \frac{Z_i}{X_{i+1} - X} \right)$$

where Δg :   Gravitational anomaly value

       G   :   Gravitation constant

       $\Delta \rho$:   Difference of density

2-2-3   Result of Prospecting

1.   Bouguer Anomaly

Gravitational distribution of the survey area is explained on the Bouguer map Plate 3, Fig. 2-5 (ρ = 2.60 g/cm^3) which is considered to reflect very well the geologic structure of the area.

The Bouguer anomalies in the survey area are distributed with a low of -142 mgal in the southern corner to a high of -122 mgal in the northern part showing a total relief of 20 mgal.

The distribution of Bouguer anomaly is as follows:

(i)   the gravity contour flows northeastward strongly reflecting the geologic structure of northeasterly trend assumed to be present in the survey area, and the gravity decreases sharply from the northwestern part toward the southeast.

(ii)   low gravity anomaly is formed in the central part of the survey area, showing an appearance to reflect the basin structure of the basement of the neighboring area, but it becomes indistinct on the northern side of the survey line No. 15, and

(iii)   along with the above, the gravity contours shift to east-west direction, leading to an estimation of the change of the basement structure in this part.

In the zone of steep inclination of gravity in the northwestern part of the survey area, the gravity contours are strongly inclined southeastward with 5 to 10 milligals per kilometer. It is thought that it reflects southeastward steep dipping of high-density basement in a general view. However, it is a general tendency of the surrounding area that gravity decreases toward the east, and it is also presumed that geologic structure would change in the deeper subsurface. It would be required to take into consideration these.

However, the extent of the survey area was too narrow to clarify the above at present.

It is also assumed in the steep dipping zone, as a matter of course, that the basement subsided by forming a fault, and that the part with the steep inclination of gravity contour may correspond to it. Therefore, it appears that those parts such as from No. 40 of the survey line 9 to No. 38 of the line 20 and from No. 38 of the line 13 to No. 28 of the line 36 would correspond to it. The direction of zone with steep inclination tends to shift to northeasterly in the northern part of the survey area and to south in the southwestern part, indicating that the basement structure would change to each direction.

The gravity anomaly at the central part of the survey area show a narrow and long low gravity zone of one to two kilometers wide and more than ten kilometers long being opened toward the southwest, in which gravity tends to decrease gradually toward the southwest. However,
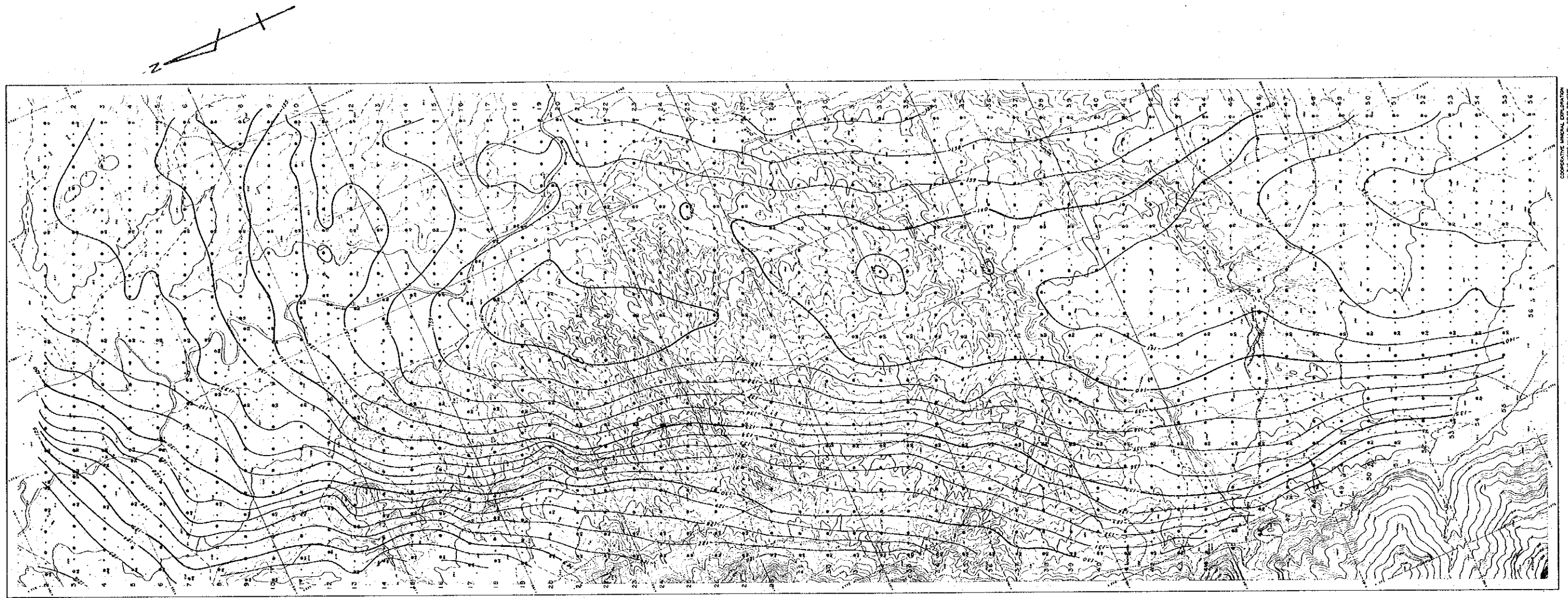
Fig. 2-5 Bouguer Anomaly Map ($\rho = 2.6\text{g/cm}^3$)

some local low gravity parts are found in the anomalous zone of low gravity mentioned in the above, such as the area centering on No. 20 of the line 18 to 26, the area including No. 4 of the line 17 to 20, No. 10 of the line 25, No. 14 of the line 32, and No. 14 of the line 36, leading to an assumption that local depression of the basement or zone of low density would occur.

2. Normal Structure

The Bouguer anomaly map includes the anomalies indicating long wave length which reflects the large-scale geologic structure at a deep part and in the surroundings of the survey area, anomalies of medium wave length reflecting faults which might be directly associated with the occurrence of ore deposits and intrusive rocks of small to medium scale, and anomalies of short wave length corresponding to noise caused by such factor as topography which can not be corrected, because of accuracy of measurement and size of the object.

Filter analysis is to detect the anomaly which consists of wave length so as to reflect very well aimed geologic structure from the various anomalies mentioned above. In this survey, the anomalies with wave length of about one kilometer was detected because the spacing of the survey lines was 250 meters and the interval of the survey stations was 200 meters and also because the scale of ultrabasic rock, in which chromite ore deposit might be emplaced, would be about 500 meters. This is shown in the residual gravity map Plate 4 and Fig. 2—6.

According to this, the positive anomalies of residual gravity are distributed in series in the zone of steep inclination of gravity in the direction of NE-SW, and anomalies were also detected in the zone of low gravity in the direction of NE-SW to NNE-SSW and in the northern part of the survey area in the direction of ENE-WSW. Some positive anomalies were detected in the southern part of the area in the direction of NW-SE, suggesting the presence of fault structure in the basement and latent intrusive rock mass of high density.

Although negative anomalies of residual gravity are distributed in a form to make a pair with the other, and it seems to reflect the depression of basement.

2—2—4　Result of Analysis

The density distribution of the rocks in the area requires to be made clear to some extent by means of drilling etc. in order to analyze quantitatively the subsurface structure from gravity distribution. Although the basement rocks are exposed in the western part, as in the survey area, where the depth of it has not been known in the eastern part and thick blanket of Quaternary sediments are deposited, the error would appear easily in quantitative analysis of the basement, in case of such tendency that a large-scale geologic structure might be reflected.
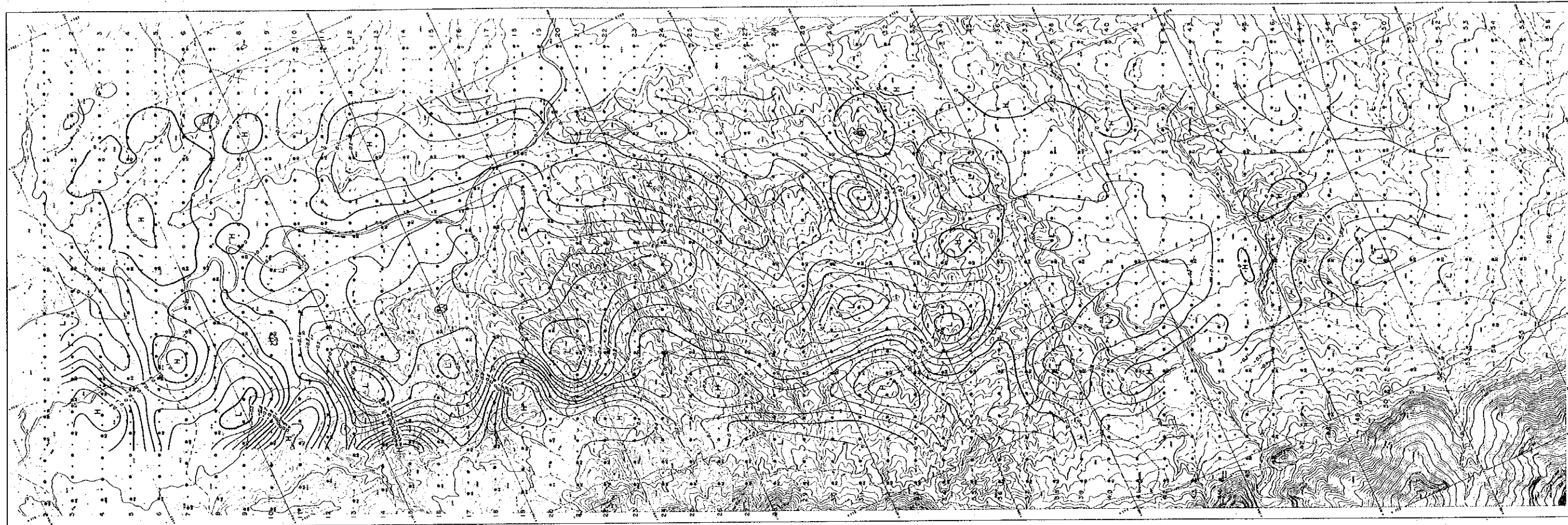
Fig. 2-6 Residual Map

Under these circumstances, the underground structure of the basement was analyzed during this survey assuming the geologic structure to be composed of two layers i.e. the basement rocks and the blanket formation overlying the former, which show the difference in density most distinctly. In this case, the average density of the basement was set to be 2.6 g/cm³ and that of the unconsolidated sediments including talus deposit, river sands and gravel of Quaternary to be 1.6 g/cm³, having made the difference of density to be 1.0 g/cm³. The basement structure in the case of 0.8 and 1.2 g/cm³ of density difference was also expressed in the analysis section, which will be instructive when the basement structure is made clear by drilling etc.

Plate 6 and 7, and Fig. 3-1 and 3-2 show the depth of basement. These show that the basement rocks are inclined toward the central part of the survey area with 10 to 20 degrees of inclination, and the 100-meter contour of the basement below the surface is in parallel with the foot of mountain where the basement rocks are exposed at a distance of one to 1.5 kilometers. The basement becomes generally depressed at the center of the survey area, and it is deeper on the southern side of the area which is as deep as 200 meters below the surface on the southern side of the survey line 27. The deepest depression of the basement in the area deeper than 250 meters was analyzed at the central part of the survey line 35 to 45 and on the eastern side of the line 48 to 52. On the other hand, some swelling and projection or geologic structure having a higher density than the surrounding area were detected in the central part of the survey area where the basement becomes generally depressed. The swelling was indicated from No. 10 of the line 12 to No. 20 of the line 30, and the projections at No. 10 of the line 6, No. 26 of the line 40, No. 30 of the line 44 and No. 16 of the line 47. These anomalies are found at the places where they are detected as the positive anomalies of residual gravity, leading to an assumption that these might indicate the latent zones of intrusive rocks of high density.

2-2-5   Compilation
(i)   The average density of the rock samples collected in the vicinity of the survey area was 2.69 g/cm³ in natural condition and 2.71 g/cm³ in wet condition except for chromite ore, and taking the cracks in the rock and the correlation between the topography and the Bouguer anomaly into consideration, it seems to be reasonable to determine the average density of the rocks in the survey area to be 2.60 g/cm³. In this connection the density of chromite ore was 3.84 g/cm³, basaltic rocks 2.80 g/cm³, serpentinites 2.69 g/cm³, and the Mozambique metamorphic rocks constituting the basement 2.57 to 3.07 g/cm³. On the other hand, although it is

cult to assume the density of the Quaternary unconsolidated sediments, it was assumed to be about 1.6 g/cm^3 because of plenty gravel contained in them. Therefore, from general point of view, it might be considered that the density structure of the survey area is composed of the two layers of the basement rocks and the blanket sediments.

(ii) The Bouguer anomalies of the survey area well reflect the geologic structure of the basement. On the western side of the area, a steeply inclined zone is formed reflecting a fault structure assumed to occur everywhere, indicating that the basement dips steeply towards south-east.

A low Bouguer anomaly is distributed in the central part of the survey area forming a narrow and long zone open to the south, suggesting that a boat shaped basin structure of the basement was formed in this part. On the other hand, in the northern part of the survey area the gravity contours swing to the east-west direction, which leads to an assumption that the geologic structure changes its trend to the direction of east to west in this part.

(iii) Among the residual gravity anomalies with wave length of about one kilometer, positive anomalies to be considered to reflect the intrusive rocks of high density and fault structures of small to medium scale were detected, which suggest the presence of a fault structure in the western part of the area and local swelling of the basement and latent mass of intrusive rocks in the central part.

(iv) It seems that the gravity basement in the survey area gradually increases its depth toward the center of the area to reach more than 250 meters below the surface. Some swellings of basement as high as several tens meters is considered to be present, which is almost consistent with the positive anomalies of residual gravity.

2—3　Magnetic Prospecting

2—3—1　Method of Prospecting

1.　Survey Planning

Plate 1 and Fig. 2—1 show the arrangement of survey point. The number of survey point was initially planned 2,155, but the points actually surveyed were 2,170.

The area surveyed was 60 square kilometers. Measurement was made at an interval of 100 meters along the survey lines set for the gravity prospecting.

2.　Magnetometer

Scintrex MP-2 type proton magnetometer was used for the prospecting.

The specification of the MP-2 type proton magnetometer is as follows:

Resolution	1 nT
Accuracy	± 1 nT
Range of measurement	20,000 — 100,000 nT (25 stages)

Proton magnetometer : —

While a fairly long time has passed since the nuclear magnetic resonance-type magnetometer was used for the measurement of geomagnetic field, manufacturing of small-size instruments and digital reading led to the effective utilization for field survey even at the steep topography.

Nuclear magnetic resonance-type magnetometer is designed to utilize gyromagnetic character of hydrogen proton, and the strength of gyromagnetic field is to be determined by the measurement of period when proton makes free precession in geomagnetic field.

Proton is found in plenty in water, kerosene and alcohol. So the coil (exciting coil) is wound around the vessel in which one of those materials has been sealed, and exciting magnetic field larger than geomagnetic field is given momentarily, which results in proton to be arranged in the direction of exciting magnetic field. Then electric current is turned off to remove exciting magnetic field, which leads to precession of proton in geomagnetic field. At this moment, next formula is given between frequency f of precession and strength of outside magnetic field Ho.

$$Ho = 2\pi f/\gamma$$

where γ is called gyromagnetic ratio (magnetic efficiency/angular momentum) and it is a physical constant to be proper to the kind of nucleus (0.26752 for proton).

Thus the frequency proportionate to geomagnetic field can be measured by the same exciting coil.

3. Magnetic Anomaly

The strength of geomagnetic field to be measured is the magnitude of the vector of geomagnetic field indifferent to the direction (scalar), and it is the synthesis of the vectors of standard field and true magnetic anomaly.

STANDARD FIELD
F

F+△FI
OBSERVED FIELD
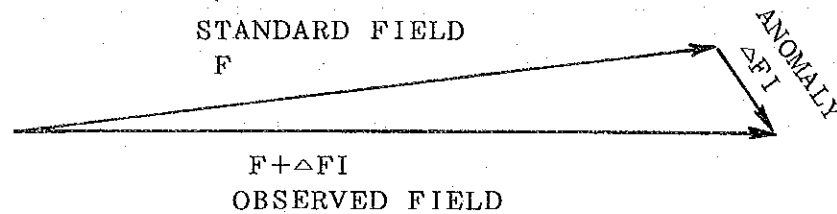
Especially in the case of surface magnetic prospecting, when magnetic anomaly is close to the magnetometer and strong, deviation of total magnetic force does not correspond to the anomaly of total magnetic force, but the form of distribution can be sufficiently examined by analysis of asymmetric anomaly caused by magnetic anomalous body.

In case the wave length of an anomaly is long, it suggests that the depth of the top of anomalous body is great or the width of it is great, and the depth, form and difference of susceptibility can be quantitatively calculated from variation of magnetic anomaly.

On the other hand, those showing short wave length reflects usually the influence of anomalous body near the surface, and especially in the case of sudden change, attention should be paid to the effect of artificial structures.

4. Correction of Diurnal Variation

In magnetic prospecting, it is sometimes necessary to correct variations such as diurnal and of short period. For example, when the period of prospecting is long and the anomaly to be measured is small and also when the prospecting is carried out at high latitude where magnetic pulse might be generated by Aurora.

In this survey, the standard point was established and magnetic observation was conducted at an interval of 15 minutes during prospecting in order to correct magnetic variation of long and short period and also to monitor magnetic storm. The results are shown in Fig. 2-7.

According to it, although the magnetic variation of short period took place in a day was less than 50 nT, that of long period during the period of the prospecting was more than 100 nT,
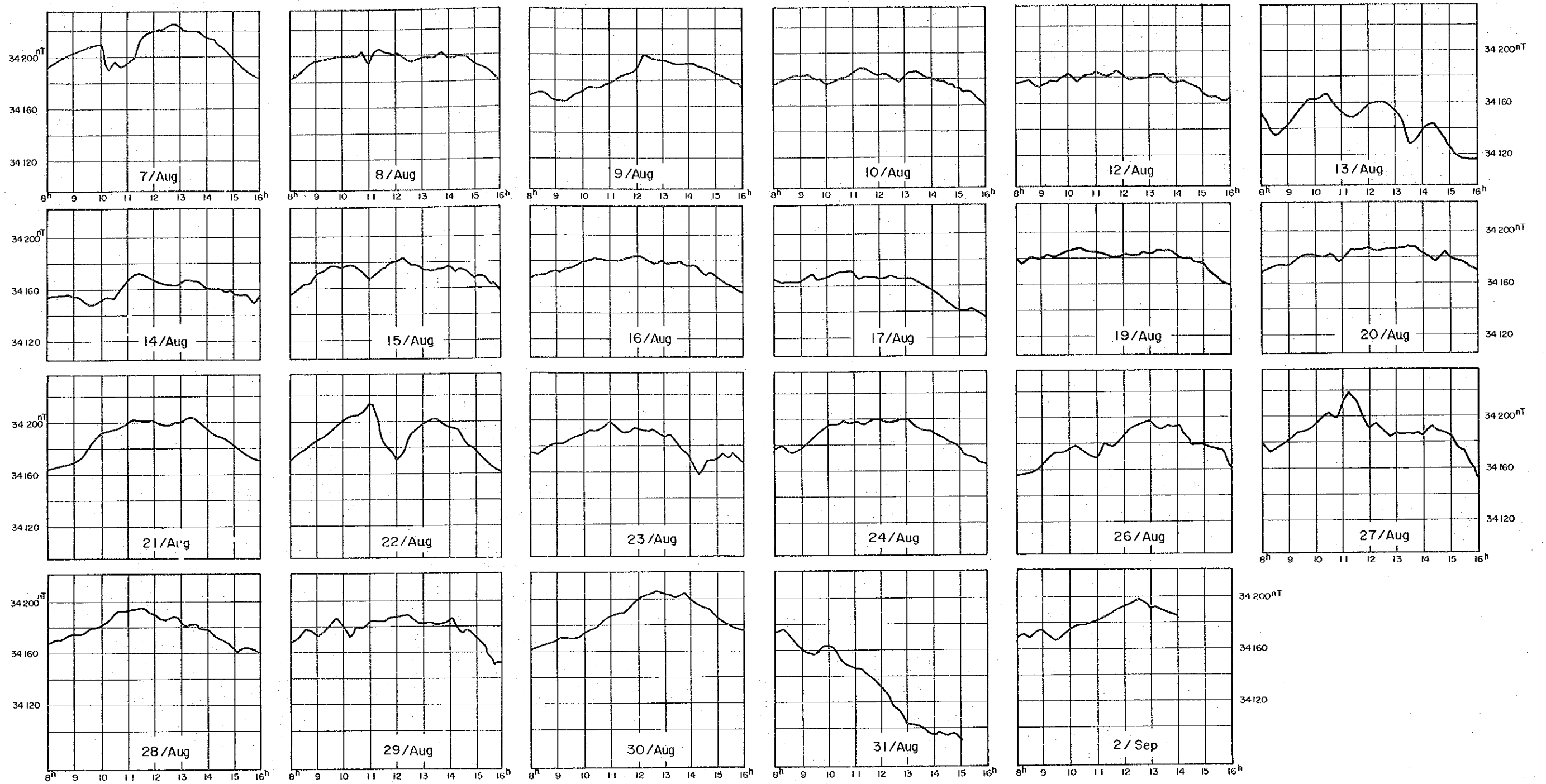
Fig. 2-7 Diurnal Variation in Wakorr (7/Aug.~2/Sep.)

Table 2—4(1) Total Magnetic Intensity at Base Station

TIME	Diurnal Variation (nt)							
	7/AUG	8/AUG	9/AUG	10/AUG	12/AUG	13/AUG	14/AUG	15/AUG
8:00	34193	34184	34168	34176	34176	34155	34156	34155
8:15	34196	34185	34169	34179	34176	34137	34156	34158
8:30	34198	34189	34170	34181	34177	34135	34155	34164
8:45	34202	34194	34170	34183	34174	34139	34157	34164
9:00	34204	34196	34164	34183	34174	34145	34155	34171
9:15	34206	34197	34166	34184	34177	34152	34154	34173
9:30	34208	34198	34166	34182	34178	34159	34148	34177
9:45	34210	34199	34169	34180	34181	34164	34148	34176
10:00	34211	34199	34172	34177	34186	34164	34152	34177
10:15	34201	34199	34175	34178	34177	34163	34155	34177
10:30	34206	34200	34175	34181	34181	34165	34155	34176
10:45	34203	34203	34176	34182	34183	34165	34159	34172
11:00	34206	34194	34178	34186	34185	34158	34166	34167
11:15	34209	34204	34181	34189	34182	34150	34171	34170
11:30	34215	34206	34184	34189	34182	34149	34172	34175
11:45	34219	34201	34186	34187	34185	34150	34169	34179
12:00	34221	34201	34188	34184	34182	34153	34168	34181
12:15	34222	34201	34199	34184	34178	34158	34165	34182
12:30	34224	34196	34198	34182	34180	34160	34164	34180
12:45	34225	34196	34196	34178	34180	34161	34164	34178
13:00	34223	34198	34194	34185	34183	34159	34164	34175
13:15	34220	34198	34195	34186	34183	34154	34167	34174
13:30	34221	34199	34193	34186	34183	34145	34166	34174
13:45	34220	34202	34192	34182	34178	34129	34165	34176
14:00	34215	34199	34192	34180	34177	34130	34162	34176
14:15	34212	34200	34193	34179	34178	34137	34161	34174
14:30	34209	34199	34190	34179	34176	34144	34160	34170
14:45	34205	34198	34188	34176	34174	34142	34158	34172
15:00	34199	34194	34186	34173	34169	34132	34159	34168
15:15	34194	34190	34184	34170	34166	34126	34155	34169
15:30	34190	34188	34182	34170	34167	34118	34156	34164
15:45	34187	34186	34178	34167	34163	34117	34150	34164
16:00	34184	34178	34176	34161	34166	34116	34155	34157
16:15		34177	34174	34156	34158	34115	34149	34149
16:30			34169	34154	34157	34113	34146	

Table 2—4 (2)   Total Magnetic Intensity at Base Station

TIME	Diurnal Variation (nt)							
	16/AUG	17/AUG	19/AUG	20/AUG	21/AUG	22/AUG	23/AUG	24/AUG
8:00	34167	34166	34180	34170	34164	34170	34176	34177
8:15	34169	34163	34176	34172	34165	34174	34174	34178
8:30	34171	34163	34179	34173	34167	34179	34176	34179
8:45	34172	34163	34181	34174	34168	34182	34178	34176
9:00	34173	34164	34181	34175	34169	34186	34182	34177
9:15	34172	34166	34183	34179	34174	34188	34182	34182
9:30	34175	34169	34182	34183	34182	34194	34186	34186
9:45	34177	34165	34184	34183	34188	34198	34186	34189
10:00	34180	34167	34185	34181	34192	34202	34189	34195
10:15	34182	34169	34187	34181	34194	34203	34190	34197
10:30	34182	34171	34187	34183	34196	34204	34192	34196
10:45	34182	34171	34185	34176	34197	34208	34195	34199
11:00	34180	34171	34185	34180	34200	34215	34198	34197
11:15	34181	34166	34184	34185	34202	34205	34196	34198
11:30	34181	34167	34182	34186	34201	34183	34187	34196
11:45	34183	34167	34181	34186	34201	34178	34192	34198
12:00	34184	34166	34182	34187	34202	34170	34194	34200
12:15	34184	34166	34183	34185	34199	34174	34192	34199
12:30	34181	34168	34182	34186	34198	34190	34192	34198
12:45	34179	34166	34184	34186	34199	34194	34192	34199
13:00	34180	34166	34183	34187	34200	34197	34190	34199
13:15	34179	34165	34185	34187	34203	34200	34186	34200
13:30	34179	34162	34186	34188	34203	34201	34187	34195
13:45	34180	34159	34186	34188	34200	34199	34181	34193
14:00	34176	34157	34184	34181	34196	34197	34174	34190
14:15	34176	34152	34180	34180	34190	34197	34171	34188
14:30	34175	34149	34181	34178	34189	34189	34159	34185
14:45	34171	34145	34177	34185	34186	34180	34160	34182
15:00	34170	34141	34175	34178	34183	34178	34169	34178
15:15	34165	34140	34170	34177	34179	34173	34168	34173
15:30	34161	34142	34166	34175	34174	34166	34175	34171
15:45	34159	34140	34160	34172	34172	34163	34172	34167
16:00	34157	34135	34158	34167	34170	34161	34169	34165
16:15	34156	34145	34157	34159	34167	34160	34166	34160
16:30	34154	34144	34155	34154	34164	34158	34160	34156

Table 2-4(3) Total Magnetic Intensity at Base Station

TIME	Diurnal Variation (nt)						
	26/AUG	27/AUG	28/AUG	29/AUG	30/AUG	31/AUG	2/SEP
8:00	34155	34179	34168	34167	34161	34174	34170
8:15	34156	34173	34170	34170	34163	34176	34171
8:30	34157	34175	34171	34177	34164	34170	34169
8:45	34159	34178	34173	34177	34166	34166	34173
9:00	34164	34182	34175	34173	34168	34161	34175
9:15	34171	34187	34175	34176	34170	34158	34168
9:30	34172	34189	34179	34181	34170	34157	34167
9:45	34173	34391	34180	34186	34171	34164	34171
10:00	34175	34197	34182	34182	34173	34164	34175
10:15	34178	34200	34187	34170	34175	34161	34178
10:30	34176	34203	34192	34178	34178	34151	34179
10:45	34169	34199	34192	34180	34184	34148	34180
11:00	34168	34213	34193	34183	34186	34145	34183
11:15	34181	34217	34194	34185	34188	34146	34184
11:30	34179	34214	34195	34184	34189	34141	34188
11:45	34177	34197	34192	34186	34195	34138	34191
12:00	34185	34191	34190	34188	34200	34132	34193
12:15	34190	34193	34186	34189	34202	34126	34196
12:30	34193	34190	34186	34189	34204	34116	34197
12:45	34195	34183	34188	34185	34206	34112	34195
13:00	34197	34186	34186	34183	34203	34102	34190
13:15	34195	34186	34182	34184	34203	34102	34192
13:30	34191	34186	34182	34181	34201	34101	34188
13:45	34194	34187	34178	34182	34204	34096	34186
14:00	34193	34180	34177	34184	34200	34094	34185
14:15	34194	34191	34174	34185	34197	34096	
14:30	34180	34189	34168	34176	34193	34095	
14:45	34178	34187	34162	34177	34192	34096	
15:00	34179	34185	34163	34174	34187	34092	
15:15	34177	34175	34163	34168	34184	34085	
15:30	34176	34173	34162	34158	34180	34078	
15:45	34174	34163	34159	34150	34177	34081	
16:00	34165	34162	34158	34152	34175	34076	
16:15	34166	34151	34157		34167	34074	
16:30	34160	34149	34157		34165	34072	

which was not so small in value. Therefore, all the measured value were corrected for diurnal variation and variation per hour.

2—3—2 Method of Analysis

The standard curves by prism, dyke and step model were produced for terrestrial magnetism (34,000 in total magnetic force and $-20°$ in inclination), and analysis was made by curve matching method with these curves and the typical magnetic anomaly curves measured.

A part of the model curves calculated were shown in Fig. 2—8, 2—9 and 2—10.

The formuals used in the analysis are shown in the following.

$$\frac{F_p(x,y,o)}{I_p} = [\cos^2 \delta \ \tan^{-1} (\frac{\alpha_1 \beta_1}{r_0 h}) - \sin^2 \delta \ \tan^{-1} (\frac{\alpha_1 \beta_1}{\alpha_1^2 + r_0 h + h^2}) + \sin \delta \cos \delta \cdot \log$$

$$(\frac{r_0 - \beta_1}{r_0 + \beta_1})] \ \Big|_{\alpha_\varrho}^{\alpha_u} \ \Big|_{\beta_\varrho}^{\beta_u} \qquad I_p = XF \qquad \delta = 90° - I$$

$$r_0^2 = \alpha_1{}^2 + \beta_1{}^2 + (h - z)^2, \ \alpha_1 = \alpha - x, \ \beta_1 = \beta - y$$

where F_p (x,y,o) :   Magnetic Anomaly (Prism)

         I_p :   intensity of magnetization

         X   :   magnetic susceptibility

         F   :   intensity of magnetic field

         I   :   inclination of the earths magnetic field

         h   :   depth below the level of observation

$$\frac{Fd(x,o,o)}{I_p} = 2 \ C \sin d \ [\sin\phi \ (\tan^{-1} \frac{x + a}{h} - \tan^{-1} \frac{x - a}{h}) + \cos\phi \ \ell n \frac{r_2}{r_1}]$$

$$C = 1 - \cos^2 I \cos^2 A \qquad \phi = 2i-d, \ i = \tan^{-1} (\tan I/\sin A)$$

where F_d (x,o,o) :   Magnetic Anomaly (Dike)

         d   :   dip angle of dike measured from horizontal

         a   :   half width of the dike

$$r_1 = \sqrt{(x + a)^2 + b^2}, \ r_2 = \sqrt{(x - a)^2 + b^2}$$

         x   :   axis perpendicular to the strike of the dike

2—3—3 Result of Prospecting

The maximum value of magnetic anomaly in the survey area was 35,637 nT at the point No. 29 of the survey line 9 and the minimum value was 32,698 nT at No. 27 of the same survey line with the difference of 2,939 nT. The average magnetic value of the area seems to be about
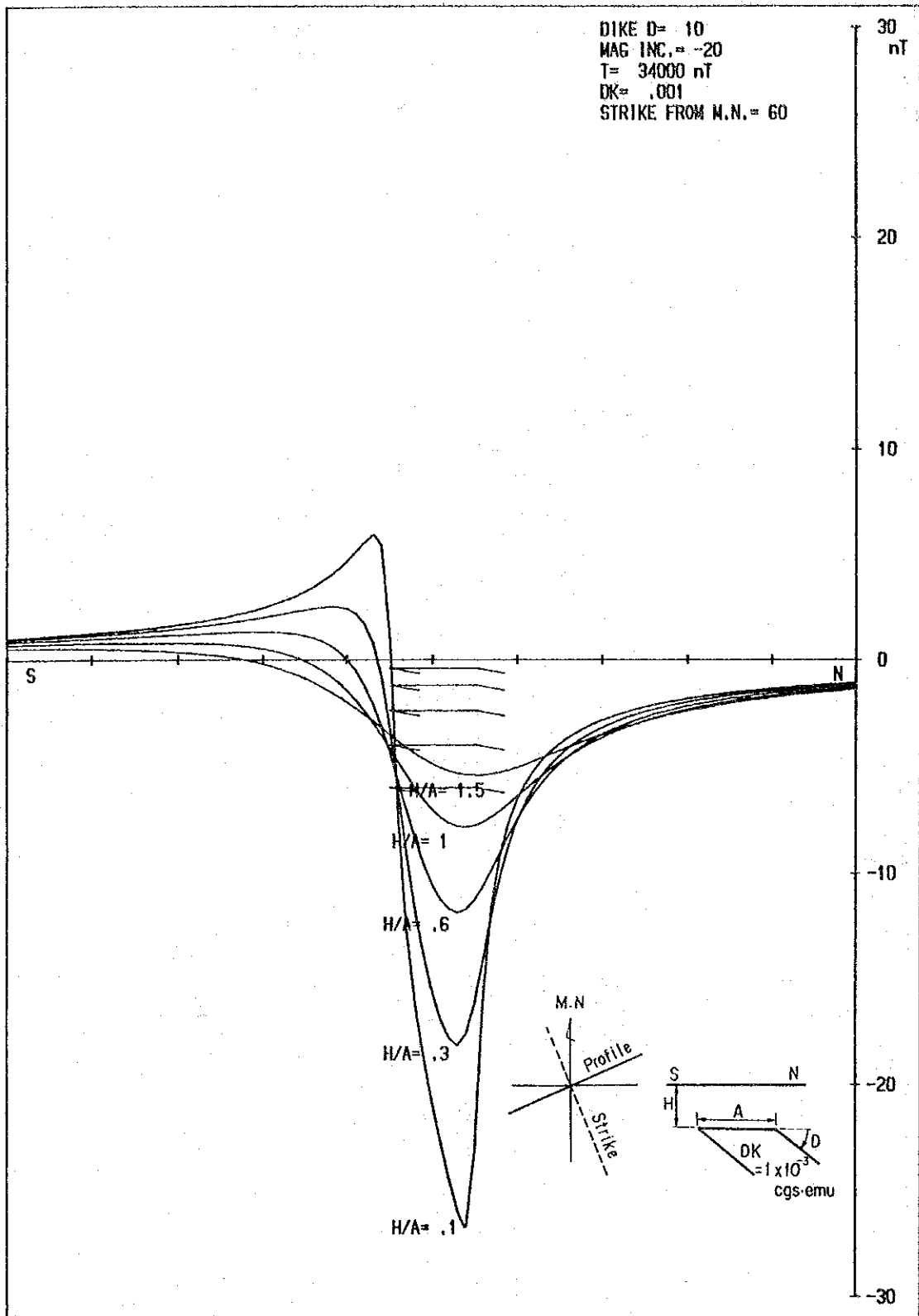
DIKE D= 10
MAG INC.= -20
T= 34000 nT
DK= .001
STRIKE FROM M.N.= 60

Fig. 2-8(1) Magnetic Anomaly due to the Two Dimensional Dyke Model
at the Inclination of −20°

DIKE D= 30
MAG INC.= -20
T= 34000 nT
DK= .001
STRIKE FROM M.N.= 60

Fig. 2-8(2) Magnetic Anomaly due to the Two Dimensional Dyke Model
at the Inclination of -20°
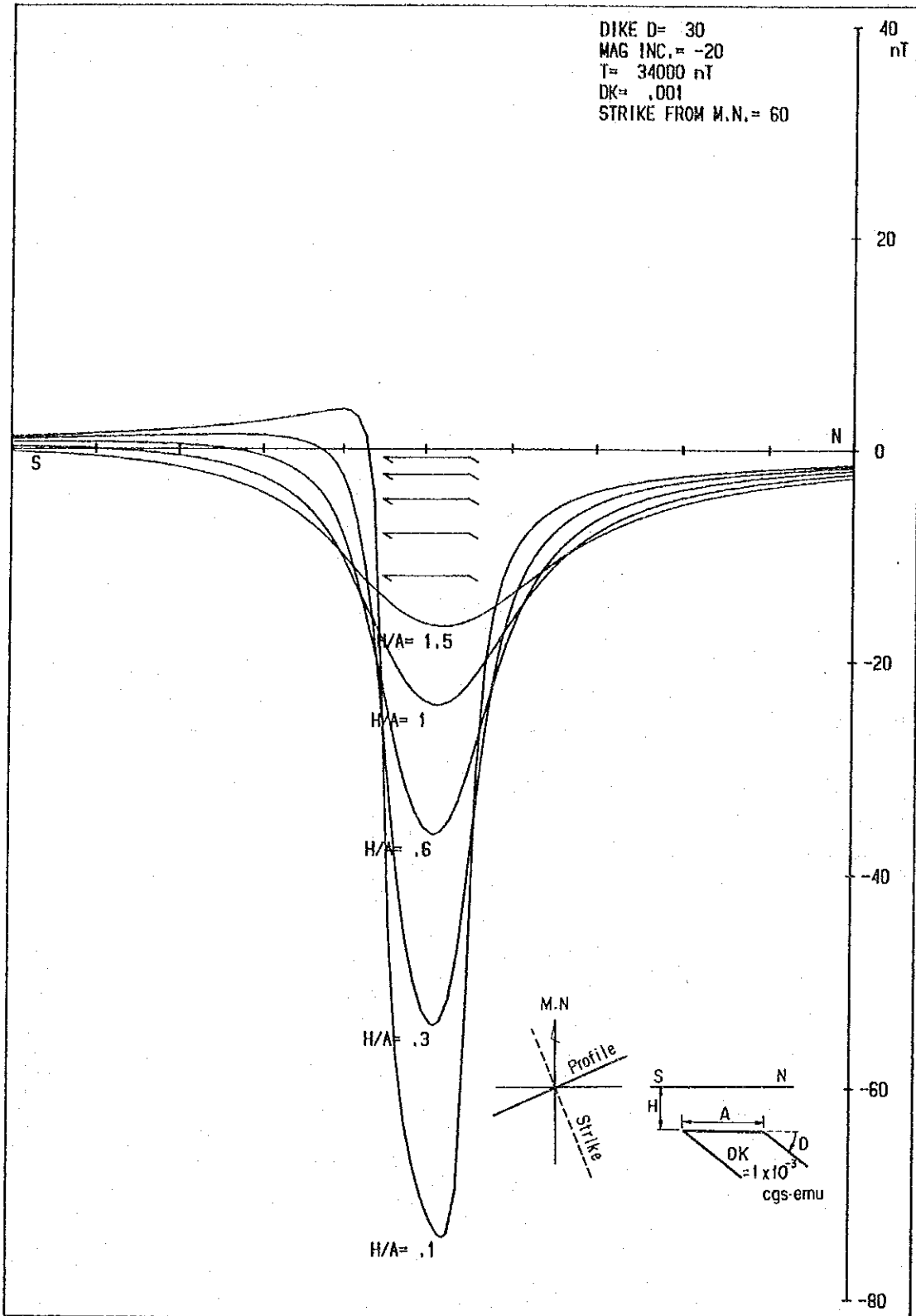
DIKE D= 90
MAG INC.= -20
T= 34000 nT
DK= .001
STRIKE FROM M.N.= 60
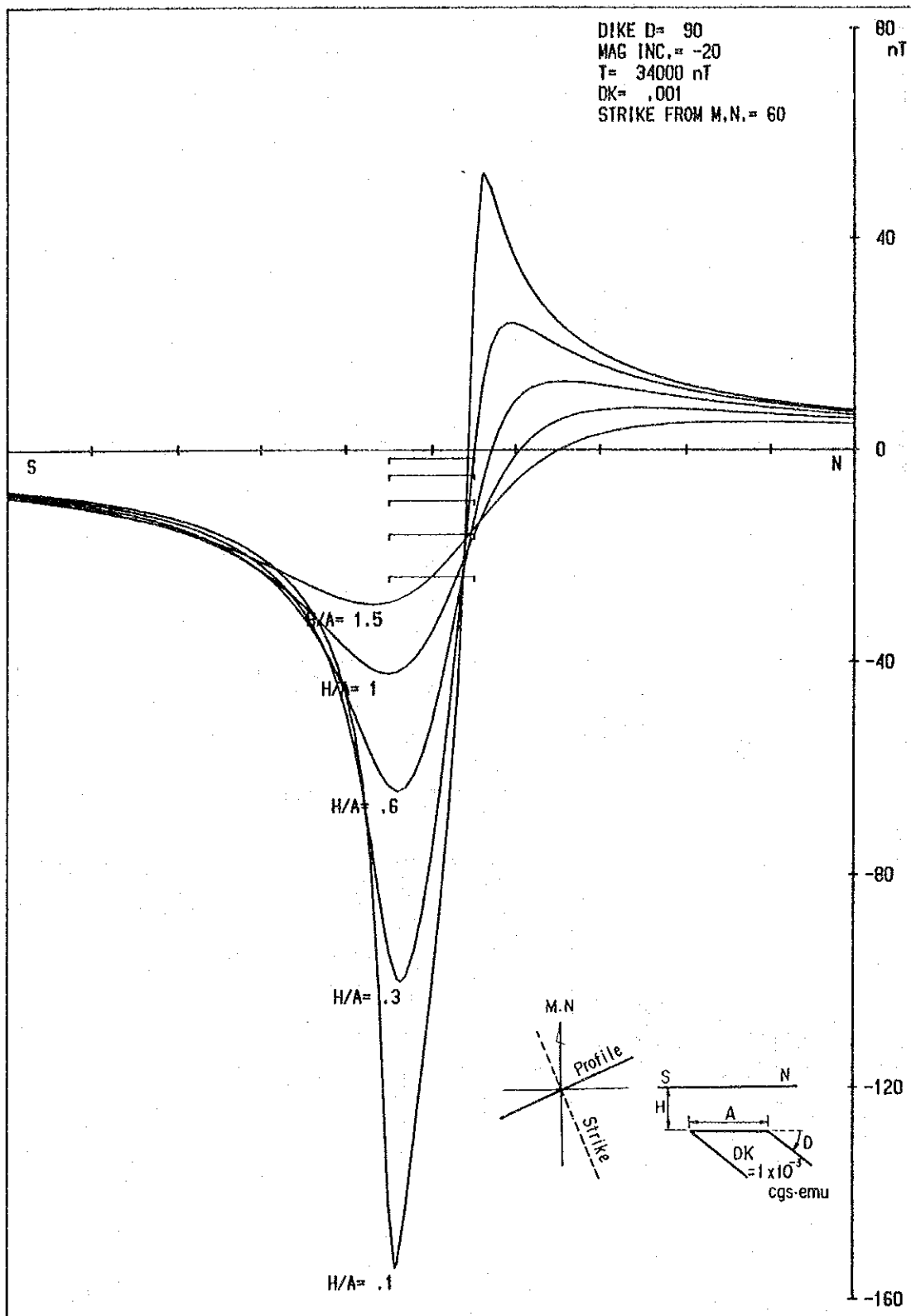
Fig. 2-8(3) Magnetic Anomaly due to the Two Dimensional Dyke Model
at the Inclination of −20°
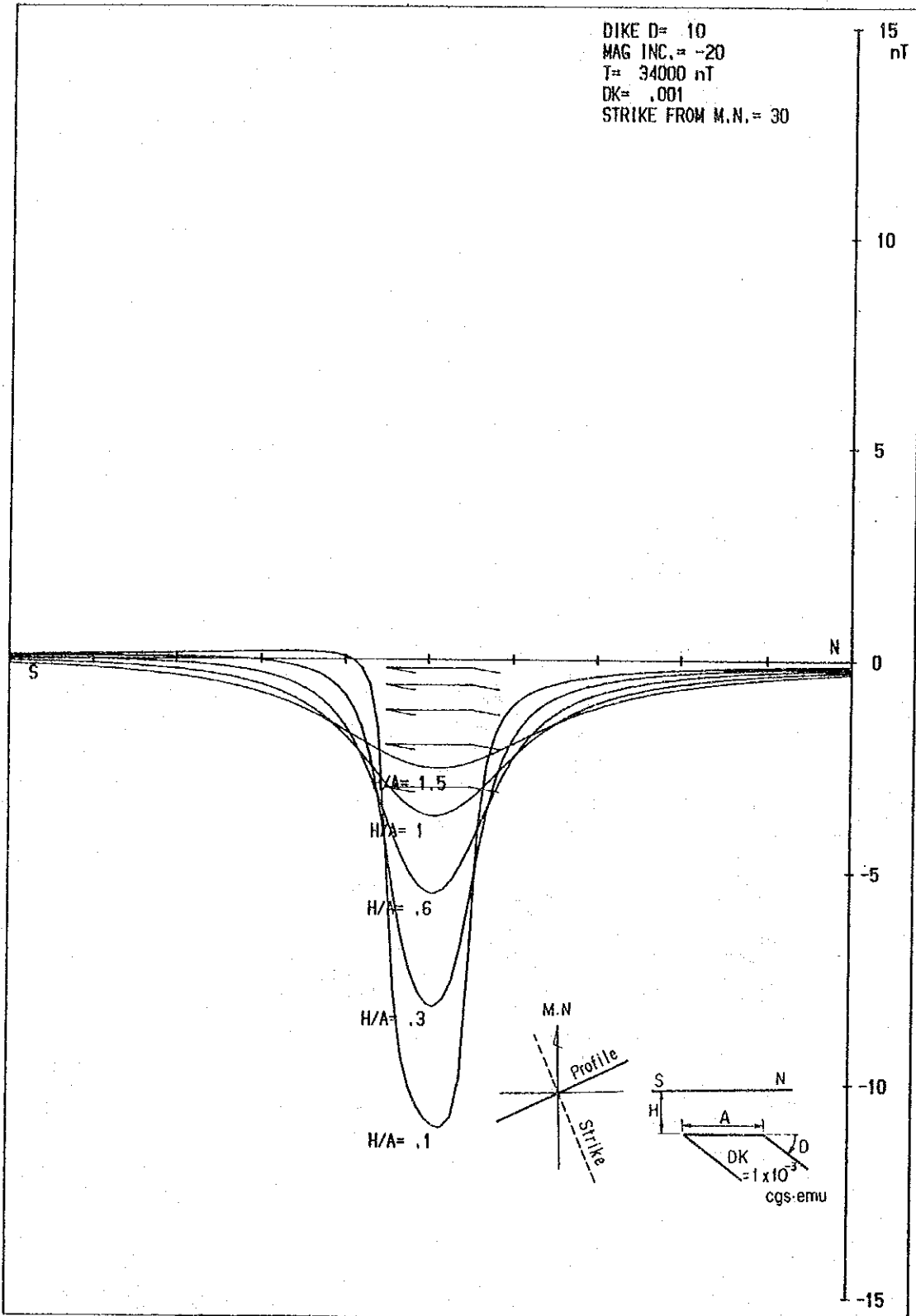
Fig. 2-8(4) Magnetic Anomaly due to the Two Dimensional Dyke Model
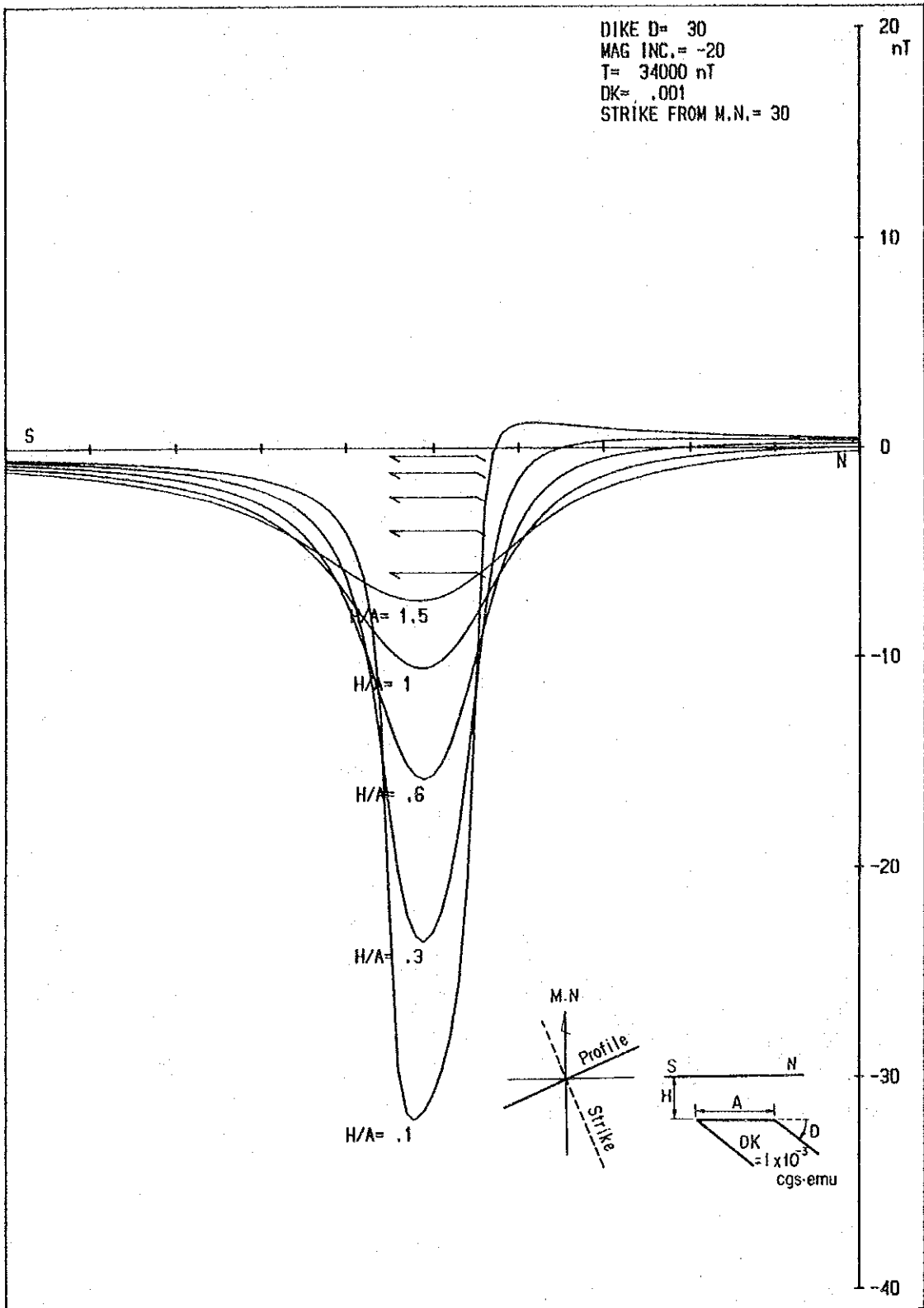at the Inclination of —20°

Fig. 2-8(5) Magnetic Anomaly due to the Two Dimensional Dyke Model
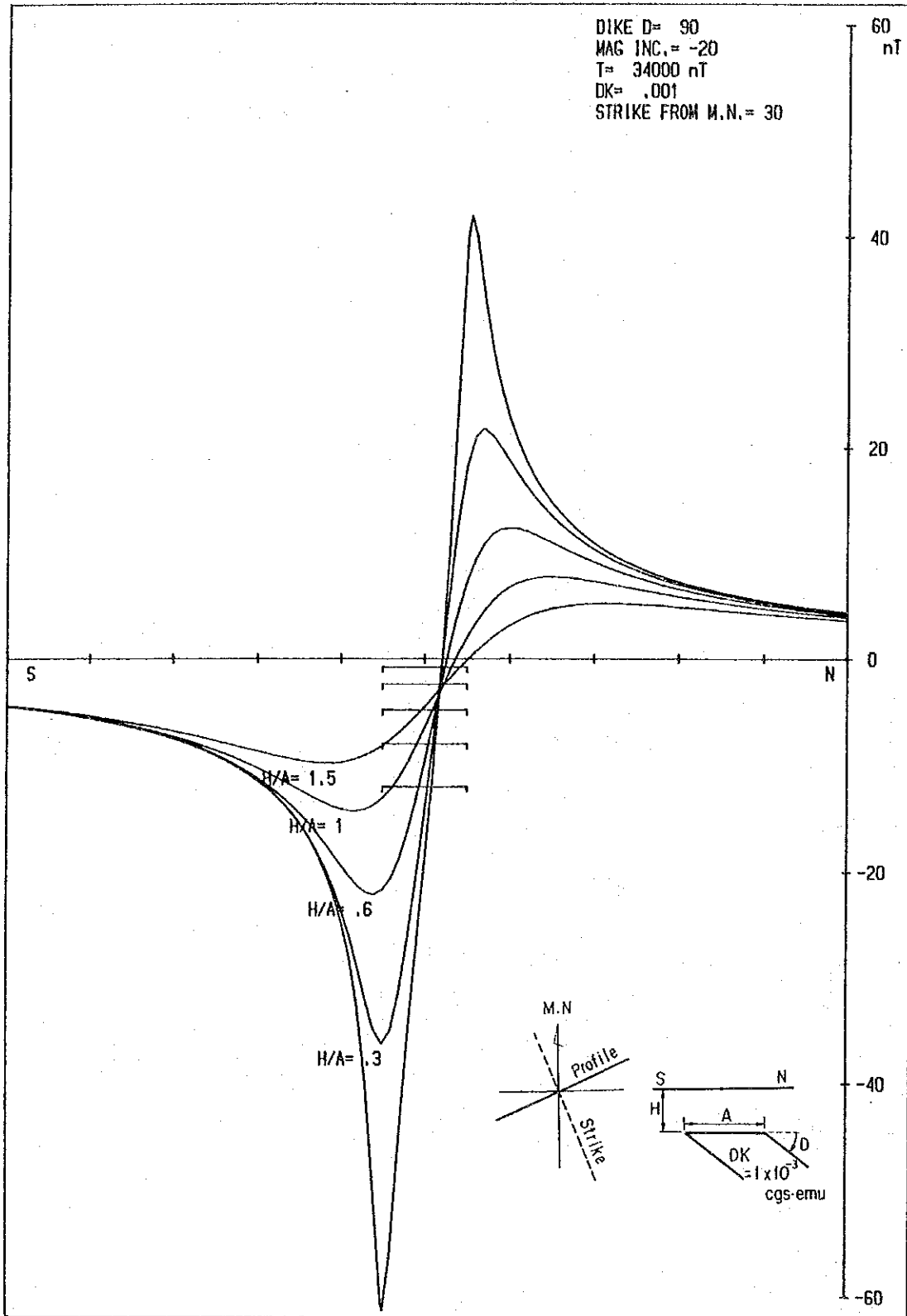at the Inclination of −20°

Fig. 2-8(6) Magnetic Anomaly due to the Two Dimensional Dyke Model
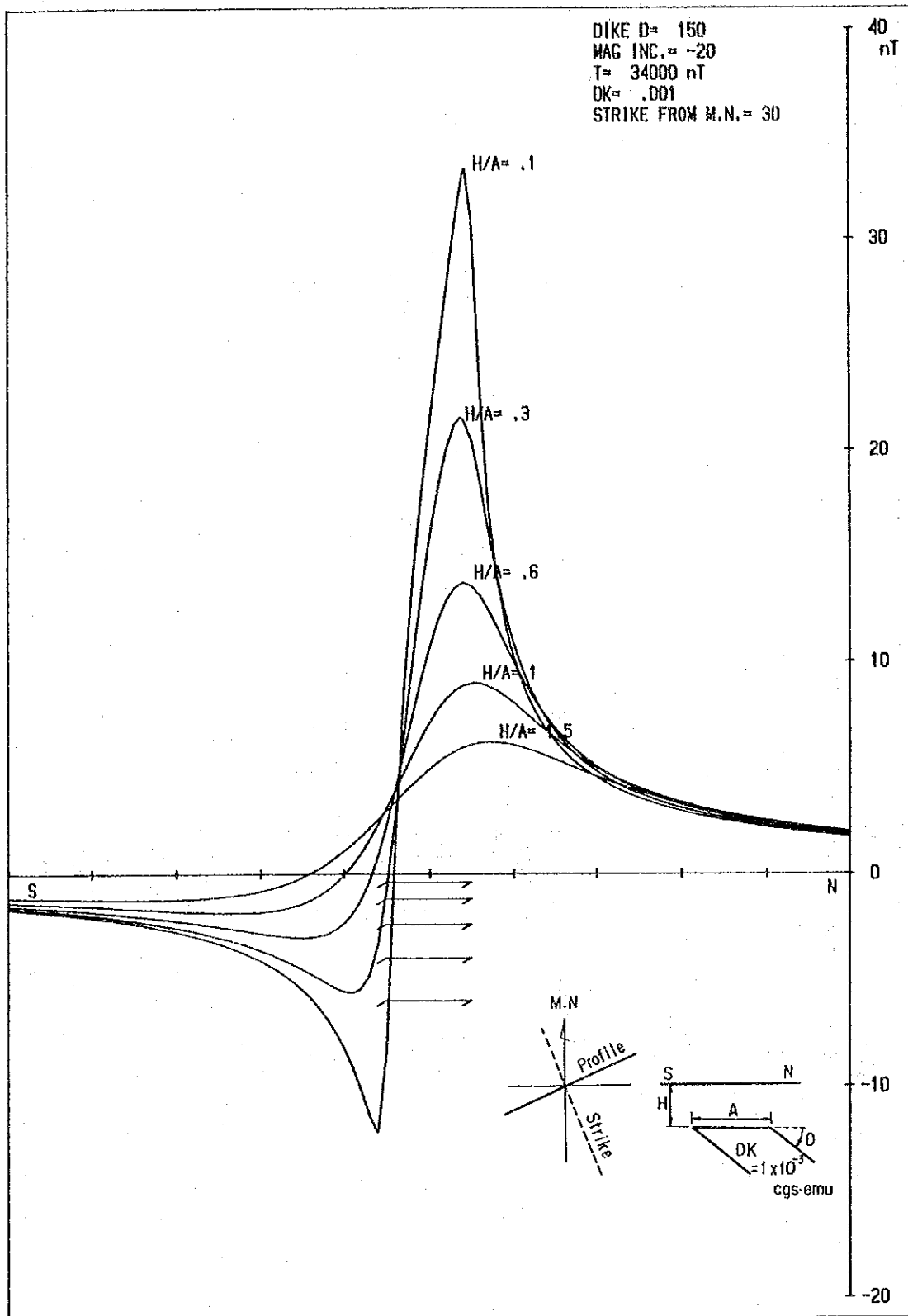at the Inclination of −20°

Fig. 2-8(7) Magnetic Anomaly due to the Two Dimensional Dyke Model
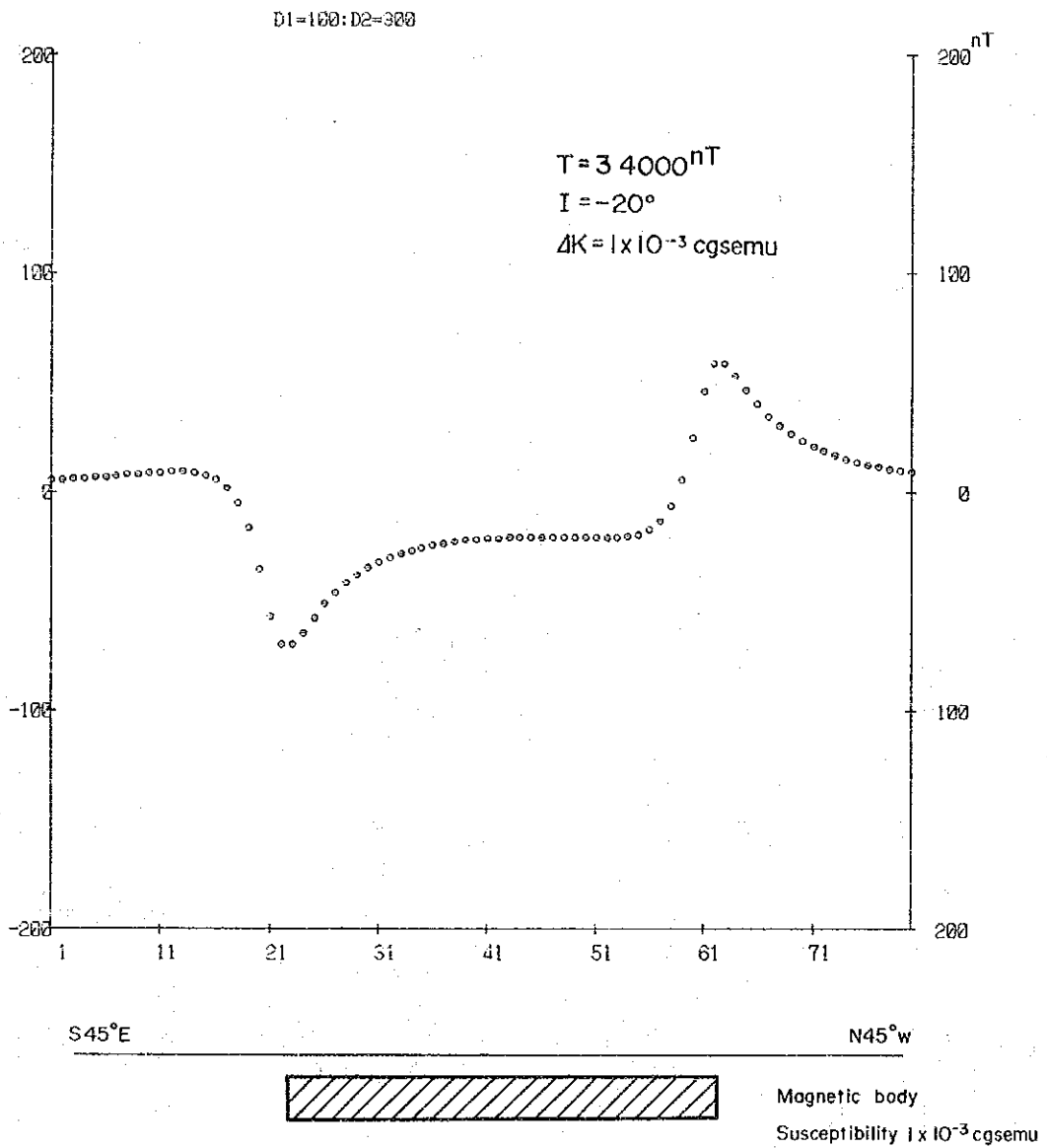at the Inclination of $-20°$

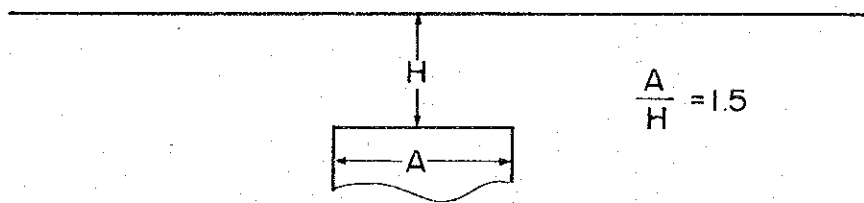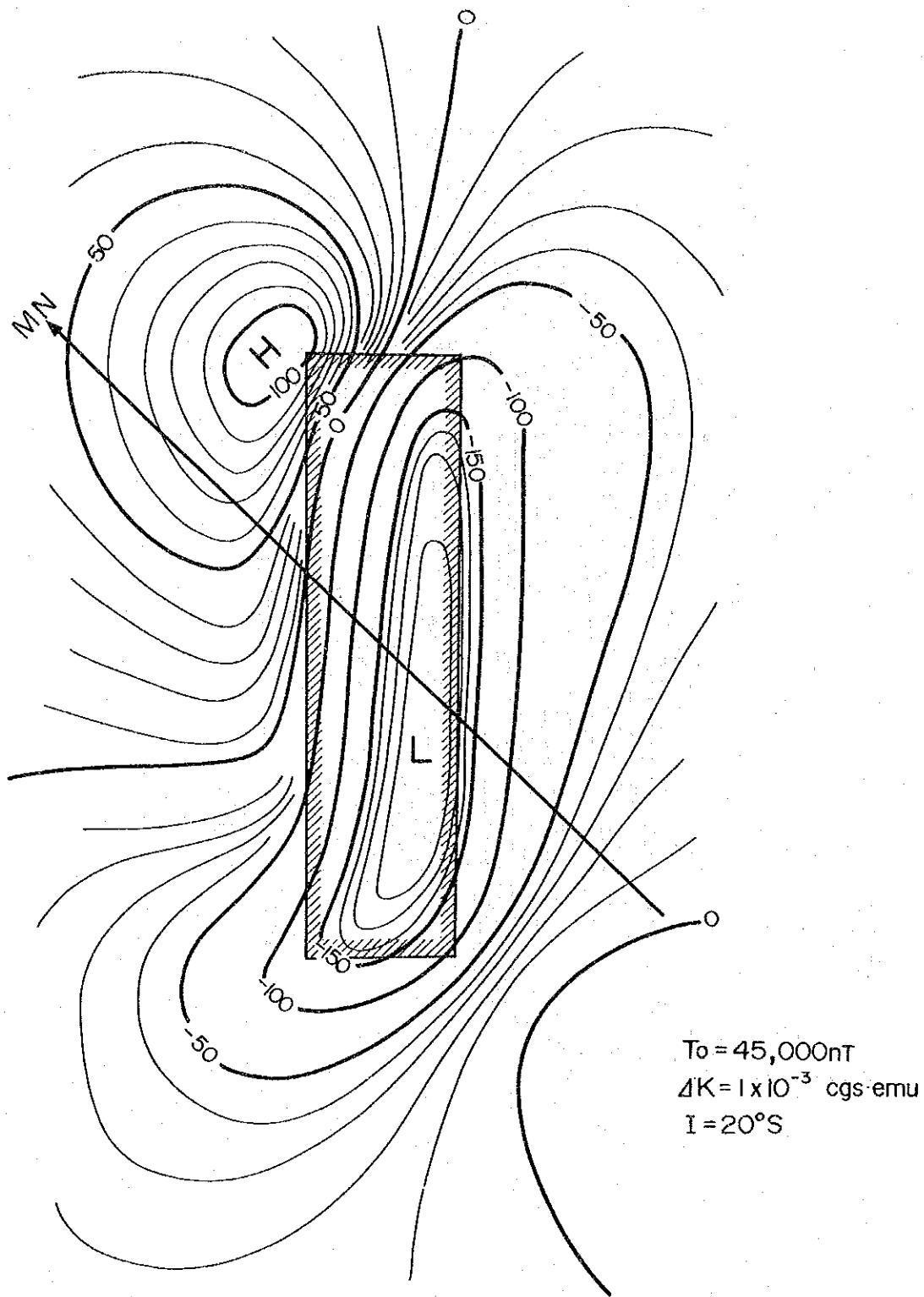Fig. 2-9(1) Magnetic Anomaly due to a Sheet Model at the
Inclination of −20°

Fig. 2-9(2) Magnetic Anomaly due to a Sheet Model at the Inclination of −20°

Fig. 2-9(3) Magnetic Anomaly due to a Sheet Model at the
Inclination of −20°

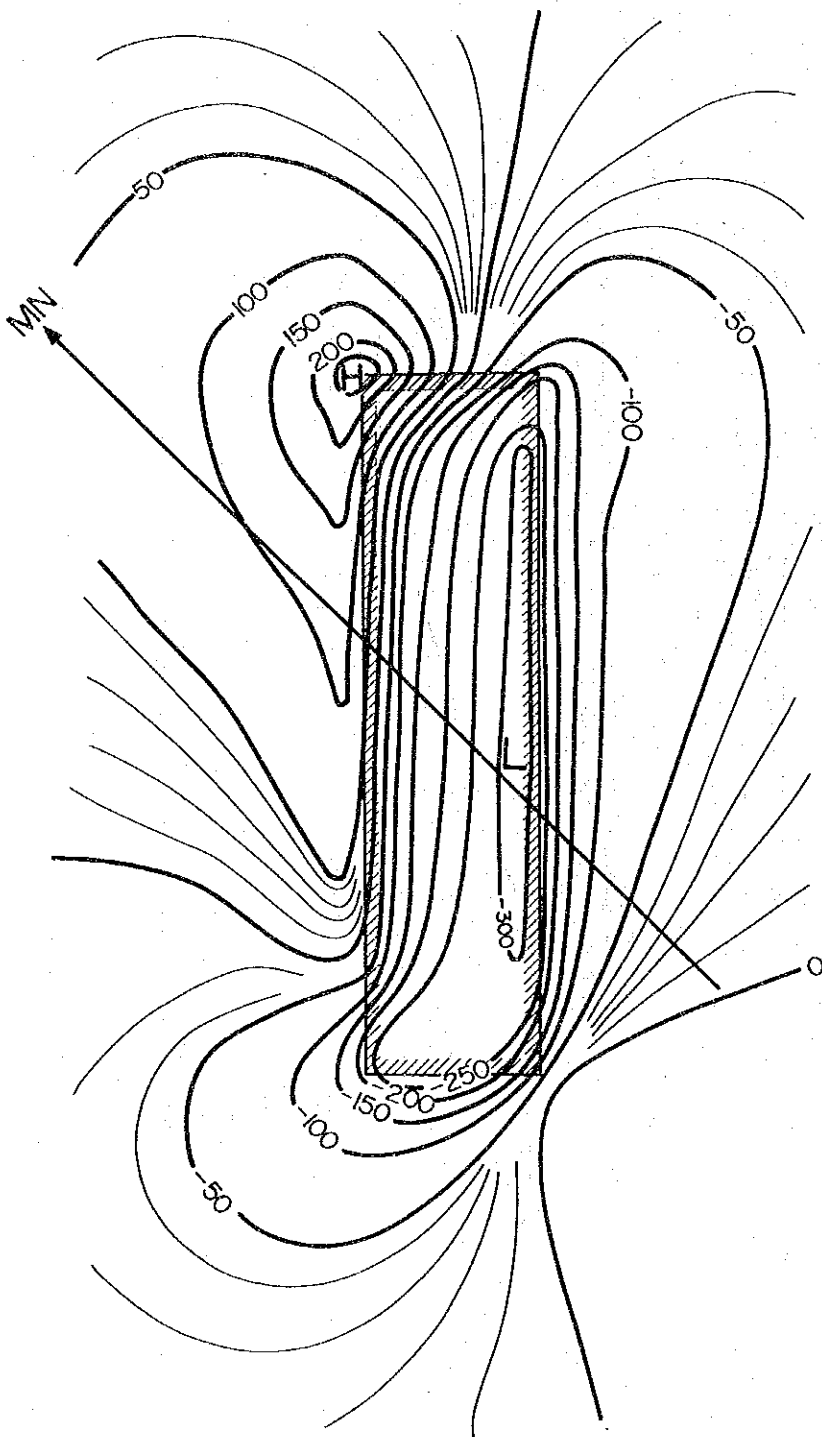To = 45,000nT
$\Delta K = 1 \times 10^{-3}$ cgs·emu
$I = 20°S$

$\frac{A}{H} = 1.5$

Fig. 2-10(1) Magnetic Anomaly due to Prism Model $(-20°)$

To = 45,000 nT

$\Delta K = 1 \times 10^{-3}$ cgs·emu
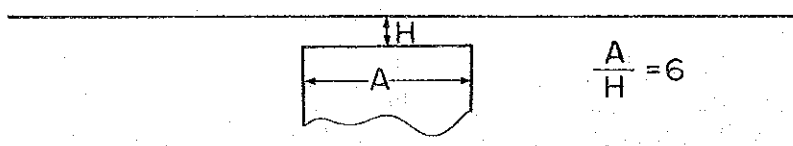
$I = 20°S$

$\dfrac{A}{H} = 6$

Fig. 2-10(2) Magnetic Anomaly due to Prism Model ($-20°$)

34,000 nT. Plate 5 and Fig. 2-11 show the distribution of magnetic anomalies.

The magnetic anomalies of short period are distributed in plenty in the survey area, especially the anomalies with amplitude of more than 500 nT were detected everywhere in the northern part of the area. However, the anomalies of short wave in the northern part are grouped in two rows being brought together, such as those from the point No. 36 of the line 12 toward the east-northeast and those from No. 20 of the line 30 toward the northeast. These groups of anomalies tend to be merged into one in the northeastern part of the survey area.

Since it is common that the strong magnetic anomaly is shown along the contact of the magnetic rock mass in such area of low magnetic latitude (20°S) as in this survey area (cf. Fig. 2-9), these series of group of anomalies seems to indicate the contact of a large magnetic rock mass.

On the other hand, in the southern part of the survey area, the groups of magnetic anomalies with maximum amplitude of about 300 nT were detected, though not so strong as compared to those in the northern part. While the group of anomalies shows a north to south trend in the northern side, it is ranged northeastward on the southern side. It is also assumed that these groups of anomalies have caught a part of the contact of a magnetic rock mass.

2-3-4 Result of Analysis

The results of analysis are shown on Plate 6, Fig. 3-1, Plate 7, Fig. 3-2 and Fig. 2-12 (1) ~ (9).

The magnetic anomalies expressed on the magnetic maps form a complicated anomalous zone consisting of high anomalies and low anomalies on a small scale. The anomalous zone detected in the northeastern part of the survey area is particularly complicated, and actually it is rather likely that the rock masses are inclined, that the susceptibility is greatly varied in local, that natural remnant magnetism (NRM) would be present and that the position of the mass is deep or shallow than that the anomalies represent a large homogeneous magnetic rock mass. The calculation of analysis of magnetism is limited in case that such a complicated magnetic distribution is shown, and the analysis is made in such a case with an assumption that these represent a large homogeneous magnetic mass.

Thus it might be a better interpretation to regard the analyzed magnetic mass to include intrusive rocks with magnetism in a rough-and-ready way.

On the other hand, if thre is no NRM detected in the magnetic rock mass in the area having a magnetic inclination of 20°S as in this survey area, positive anomaly will be shown at the contact on the northern side and negative anomaly on the southern side (cf. Fig. 2-10). The
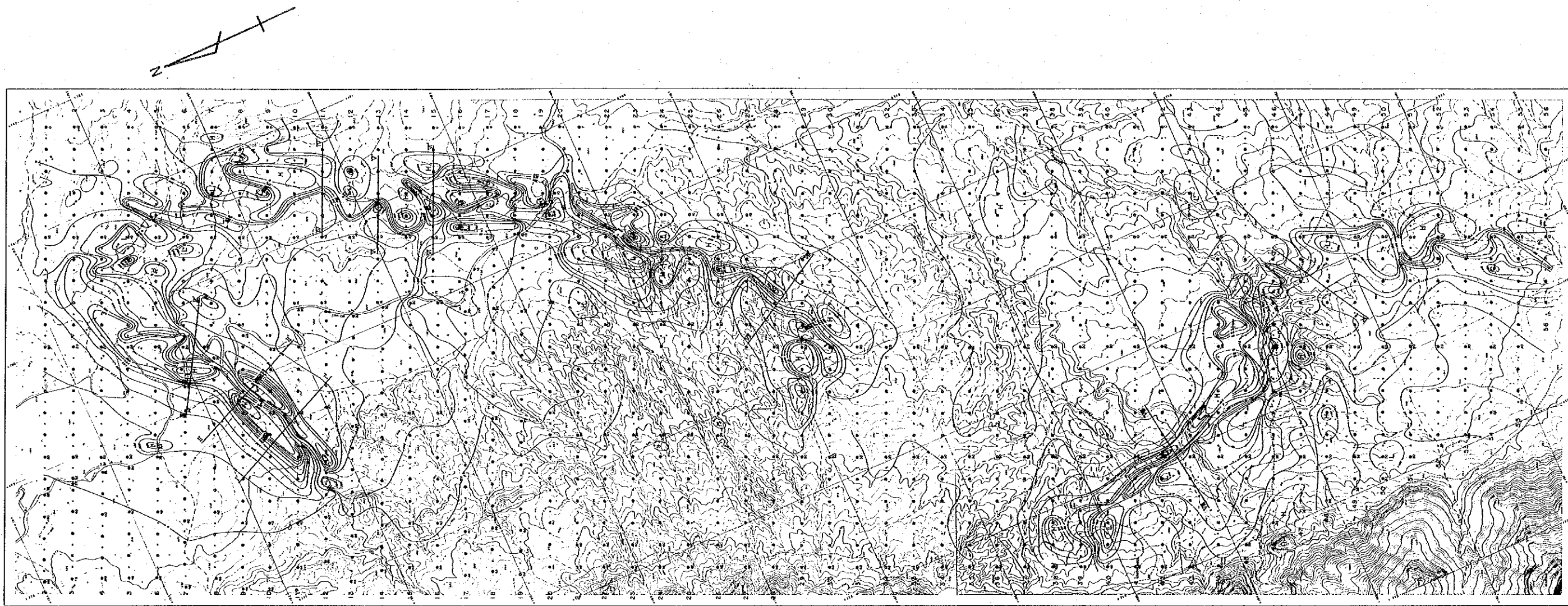
Fig. 2-11 Total Magnetic Intensity Map

Profile I

LEGEND

o------o Observed Curve

∿ Calculated Curve

7777777 Topography

▨ Magnetic Body

Δk Calculated Susceptibility
of Magnetic Body.

Fig. 2-12(1) Principal Profile of the Magnetic Anomaly

Fig. 2-12(2) Principal Profile of the Magnetic Anomaly

Profile Ⅲ

35,000 —

34,000 —

33,000 —

Ⅲ N 60° E

S 60° W Ⅲ′

30°

△k = 6.6 x 10⁻²

0
— 100ᵐ
— 200
— 300

LEGEND

o------o   Observed Curve

~   Calculated Curve

/////////   Topography

▨   Magnetic Body

△k   Calculated Susceptibility
          of Magnetic Body

Fig. 2-12(3) Principal Profile of the Magnetic Anomaly

Profile IV

Fig. 2-12(4) Principal Profile of the Magnetic Anomaly

Profile Ⅴ

34,000^{nT}

33,500

Ⅴ
N60°E

Ⅴ'
S60°W

11 10 9 8 7 6 5

0

-- 100

-- 200

-- 300^{m}

10°

$\Delta k = 11 \times 10^{-2}$

LEGEND

o-----o   Observed Curve

⌒⌣   Calculated Curve

⊿⊿⊿⊿   Topography

▱   Magnetic Body

Δk   Calculated Susceptibility
       of Magnetic Body

Fig. 2-12(5) Principal Profile of the Magnetic Anomaly

Profile VI

Fig. 2-12(6) Principal Profile of the Magnetic Anomaly

Profile Ⅶ

LEGEND

o----o   Observed Curve

⌒⌒   Calculated Curve

⊤⊤⊤⊤⊤⊤   Topography

▨▨   Magnetic Body

Δk   Calculated Susceptibility
          of Magnetic Body
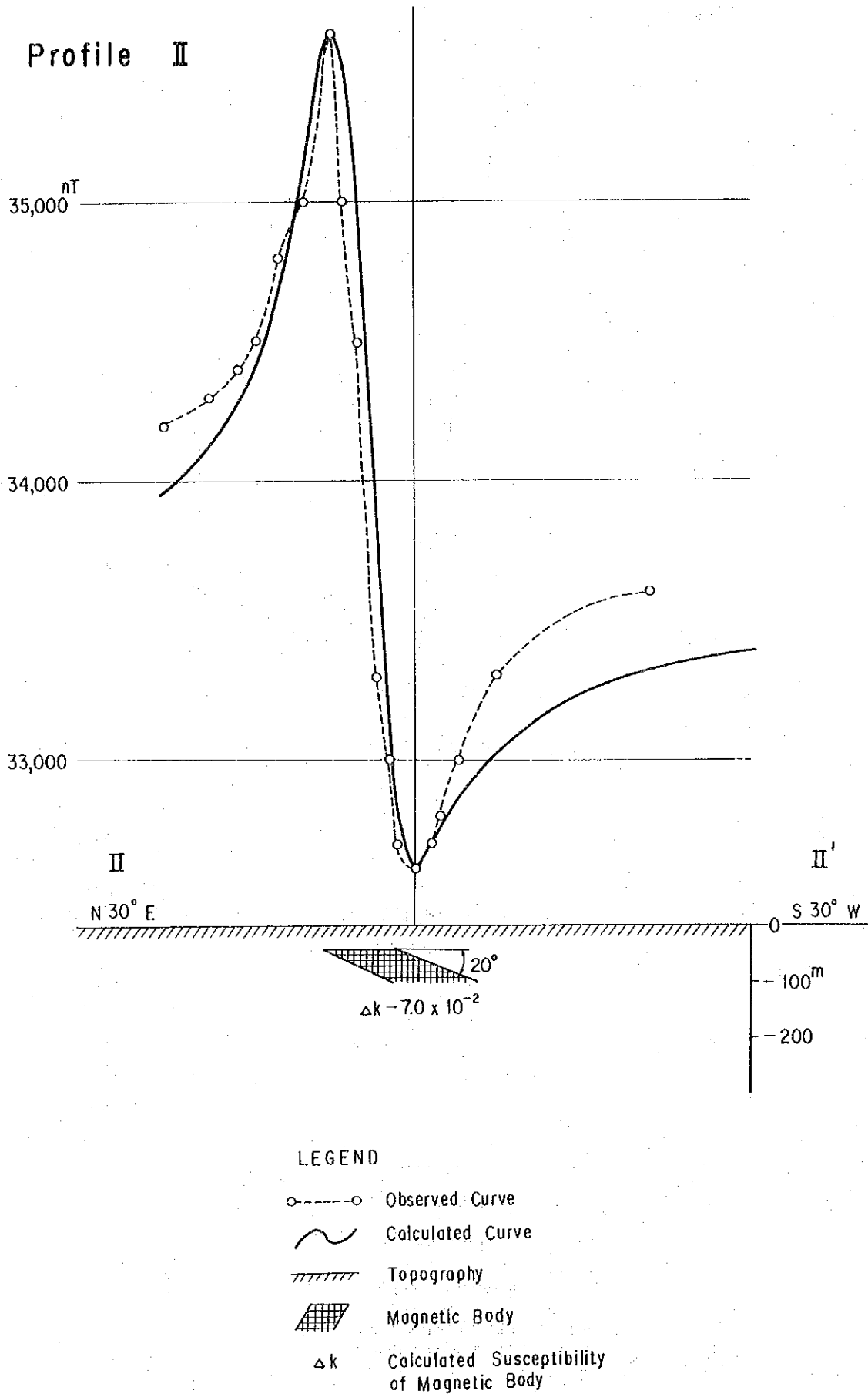
Fig. 2-12(7) Principal Profile of the Magnetic Anomaly

Profile VIII

34,000 nT

33,900

33,800

VIII E   W VIII'

10°

0

—100

—200

—300 m

Δk = 14 × 10⁻²

LEGEND

o------o   Observed Curve

⌒⌒   Calculated Curve

⁷⁷⁷⁷⁷⁷   Topography

▨▨   Magnetic Body

Δk   Calculated Susceptibility
            of Magnetic Body
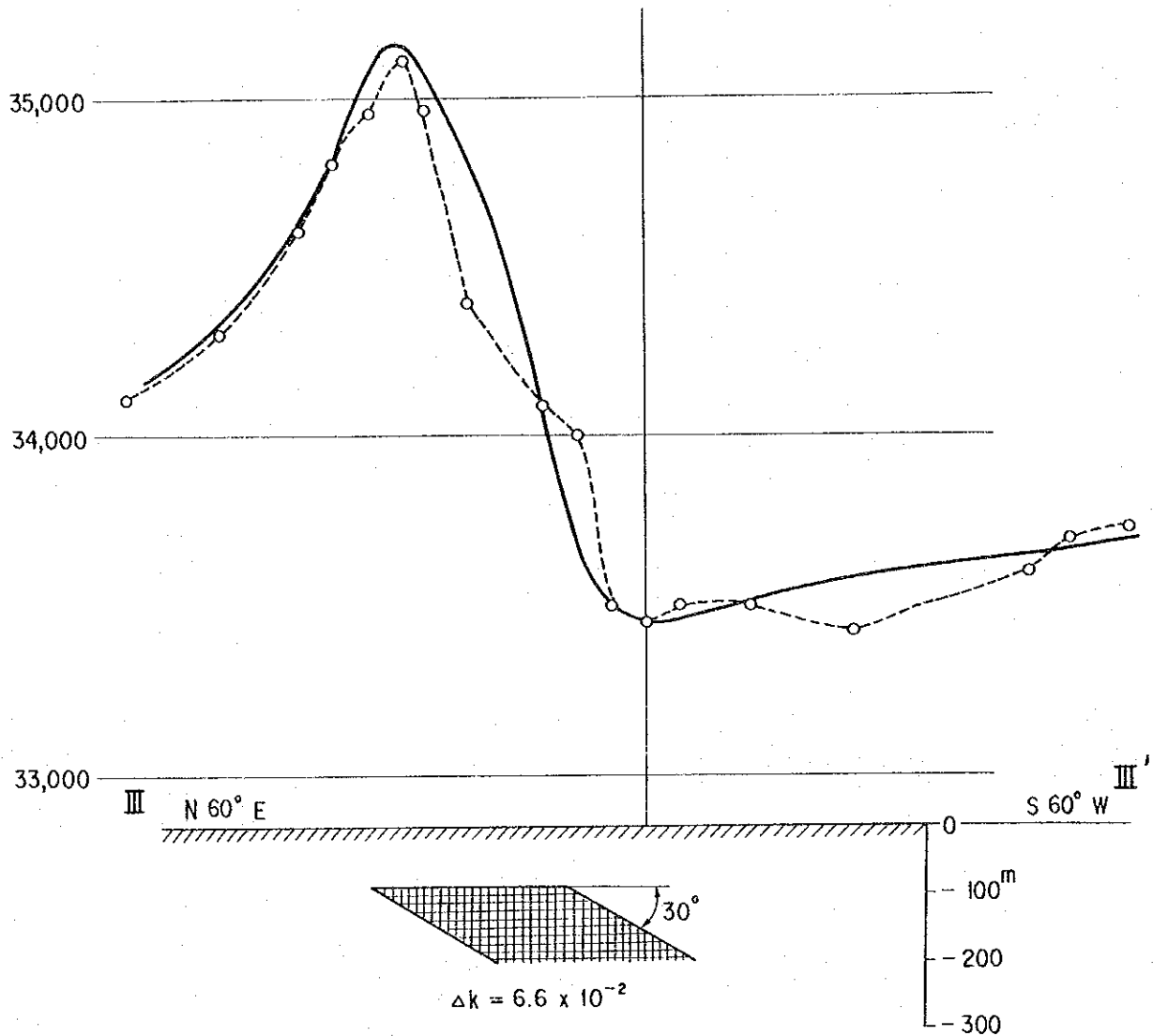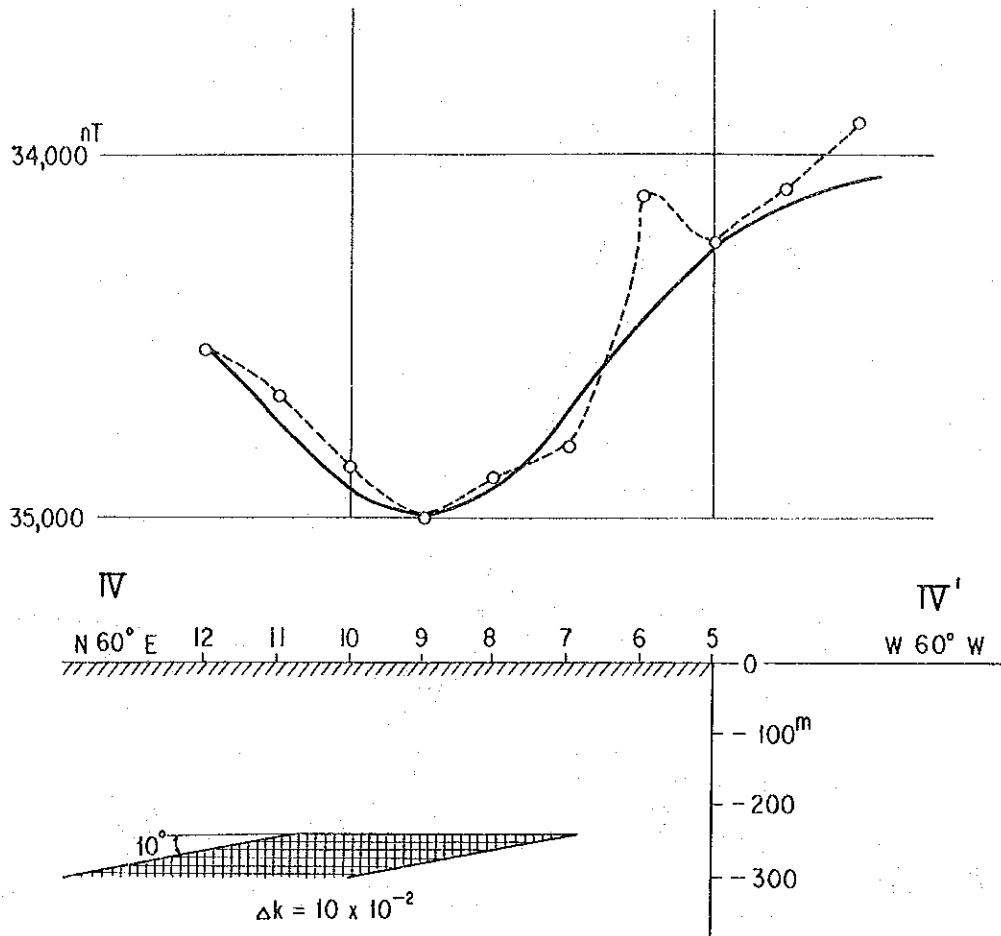
Fig. 2-12(8) Principal Profile of the Magnetic Anomaly

Profile IX

33,900 nT

33,850

33,800

IX

S 60° E

IX'

N 60° W

0

−100 m

−200

−300

60°

$\triangle k = 5 \times 10^{-3}$

LEGEND

○----○ Observed Curve

~ Calculated Curve

///// Topography

▨ Magnetic Body

△k Calculated Susceptibility
of Magnetic Body
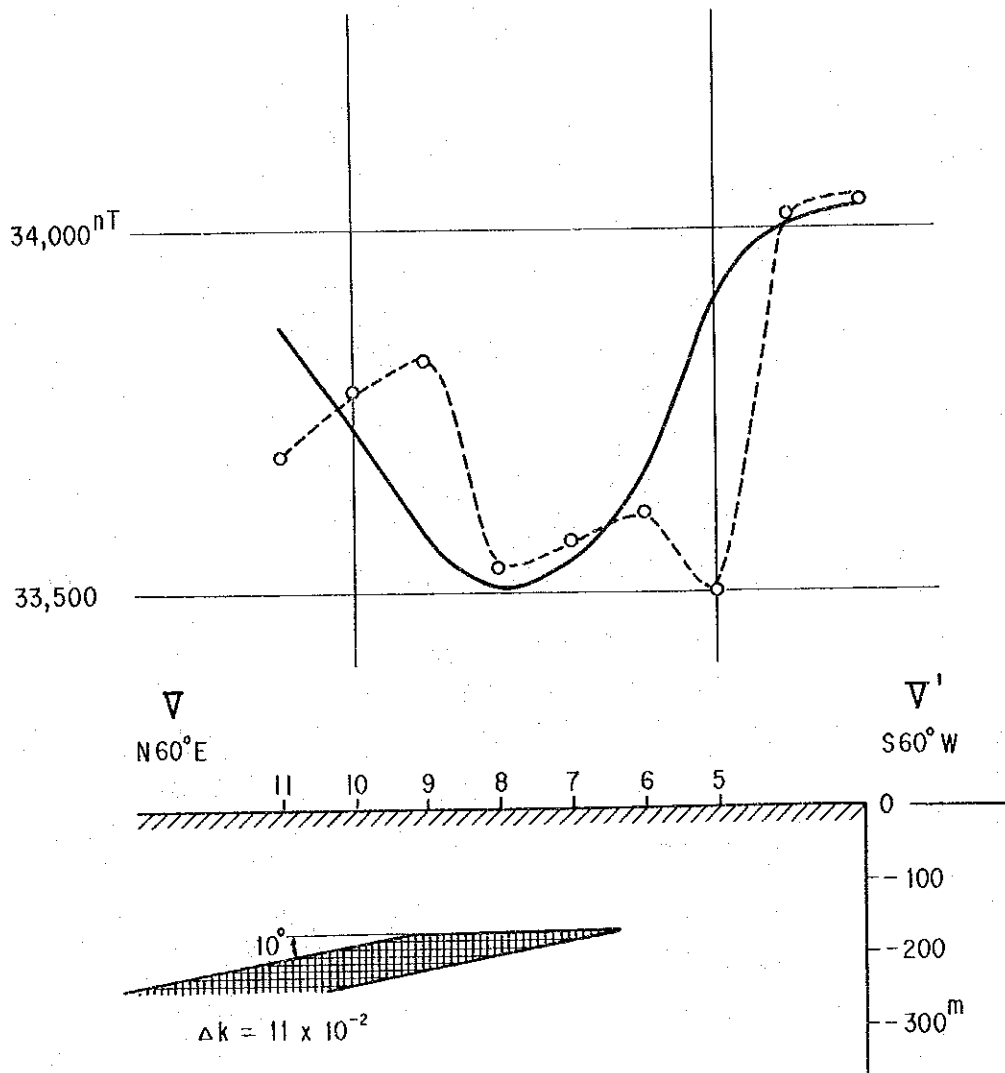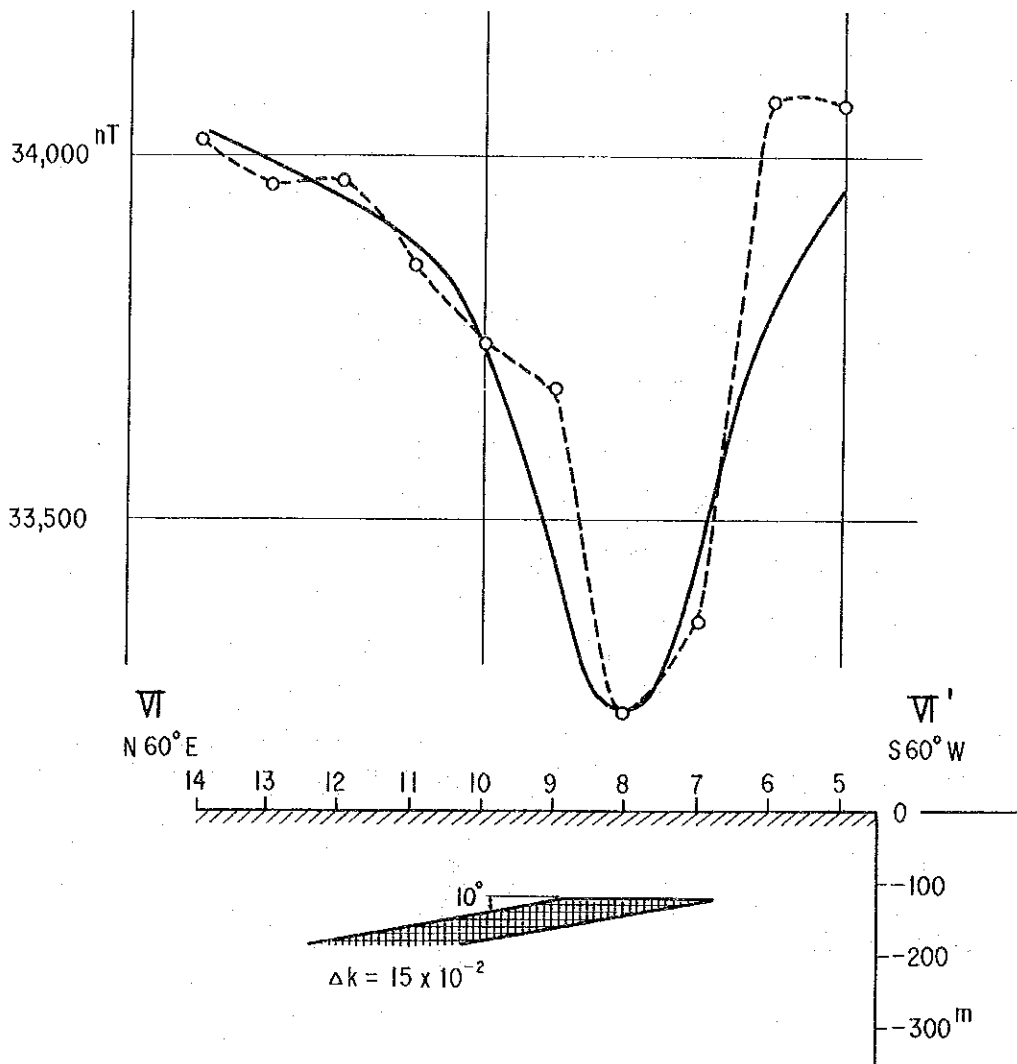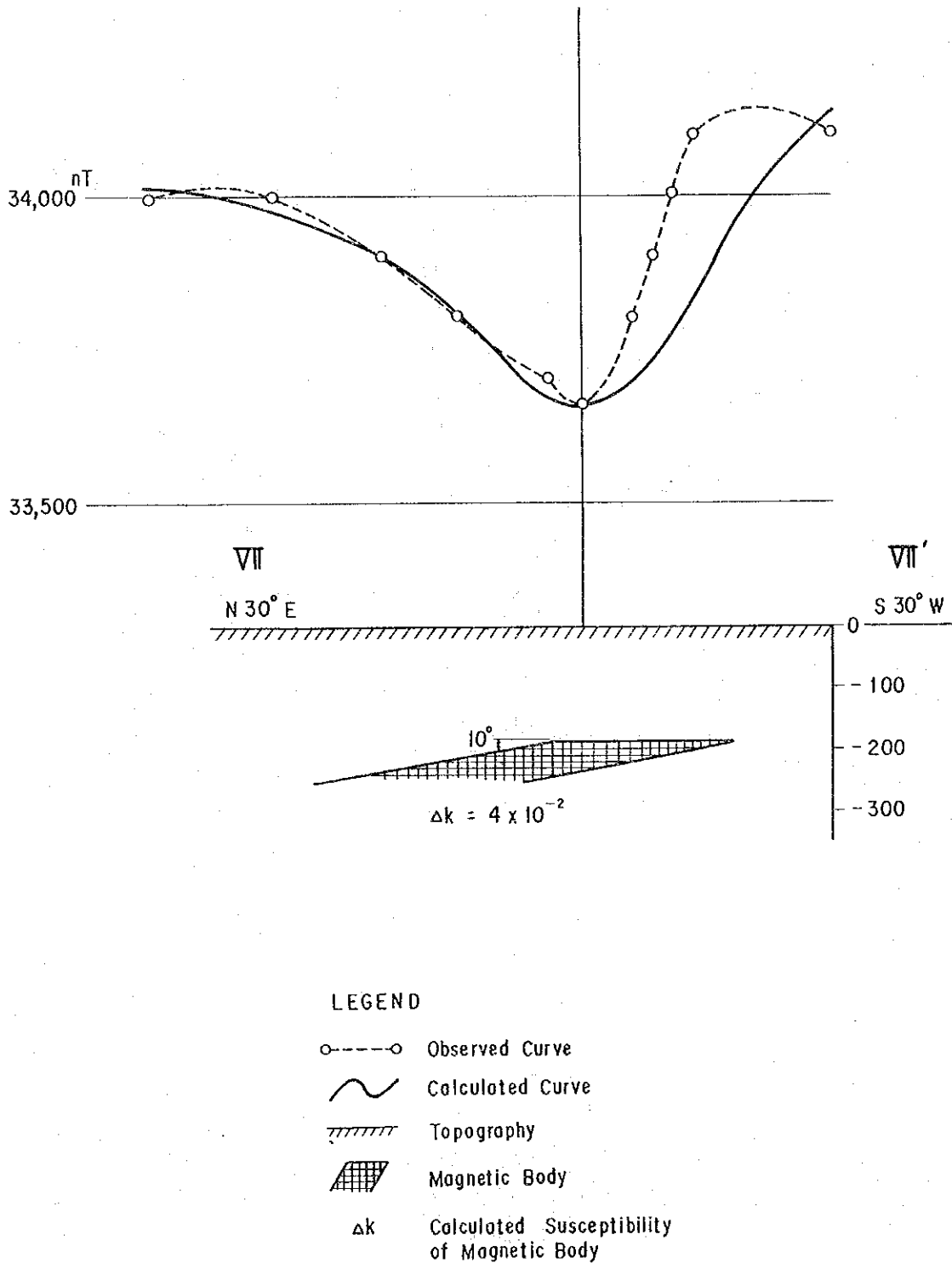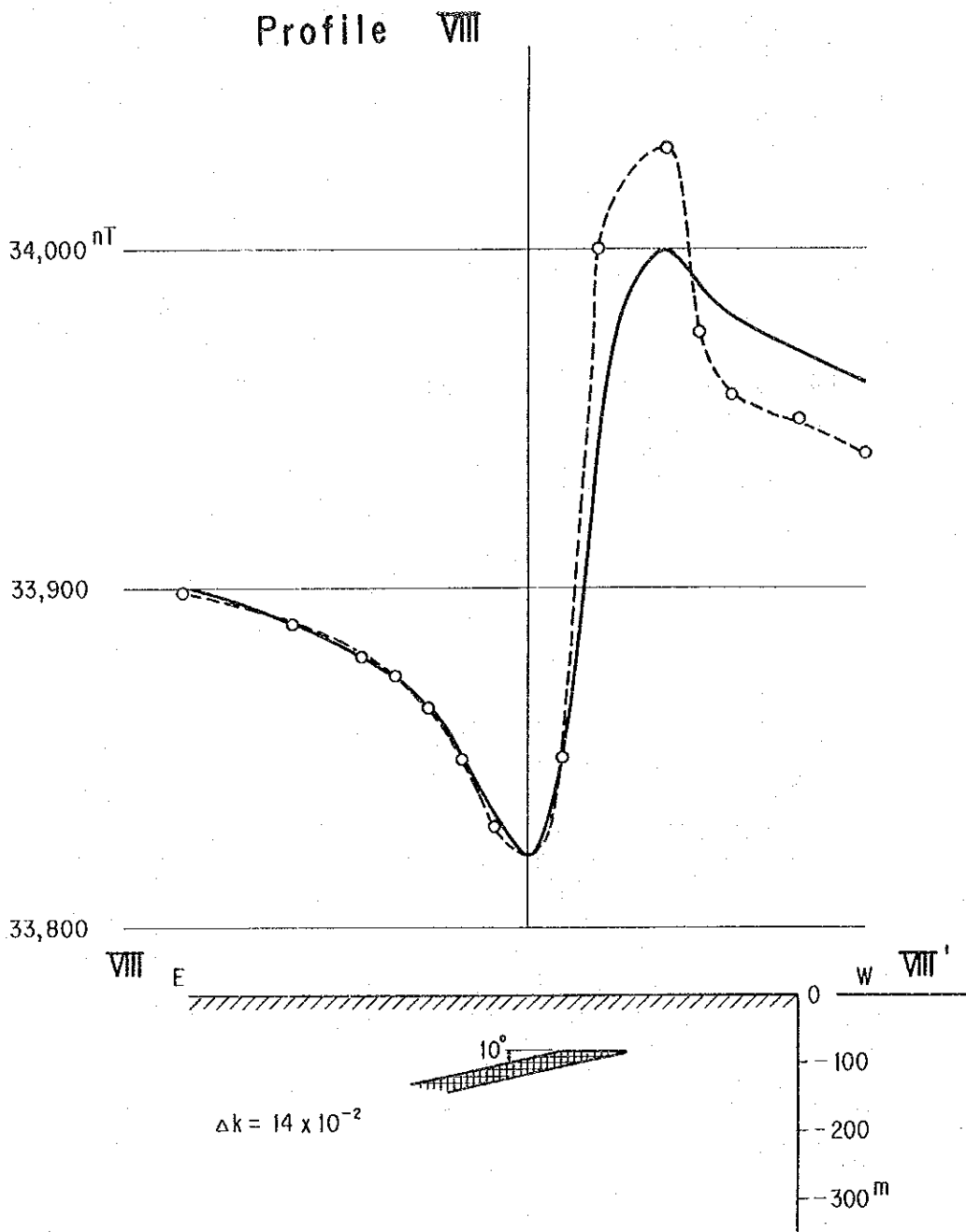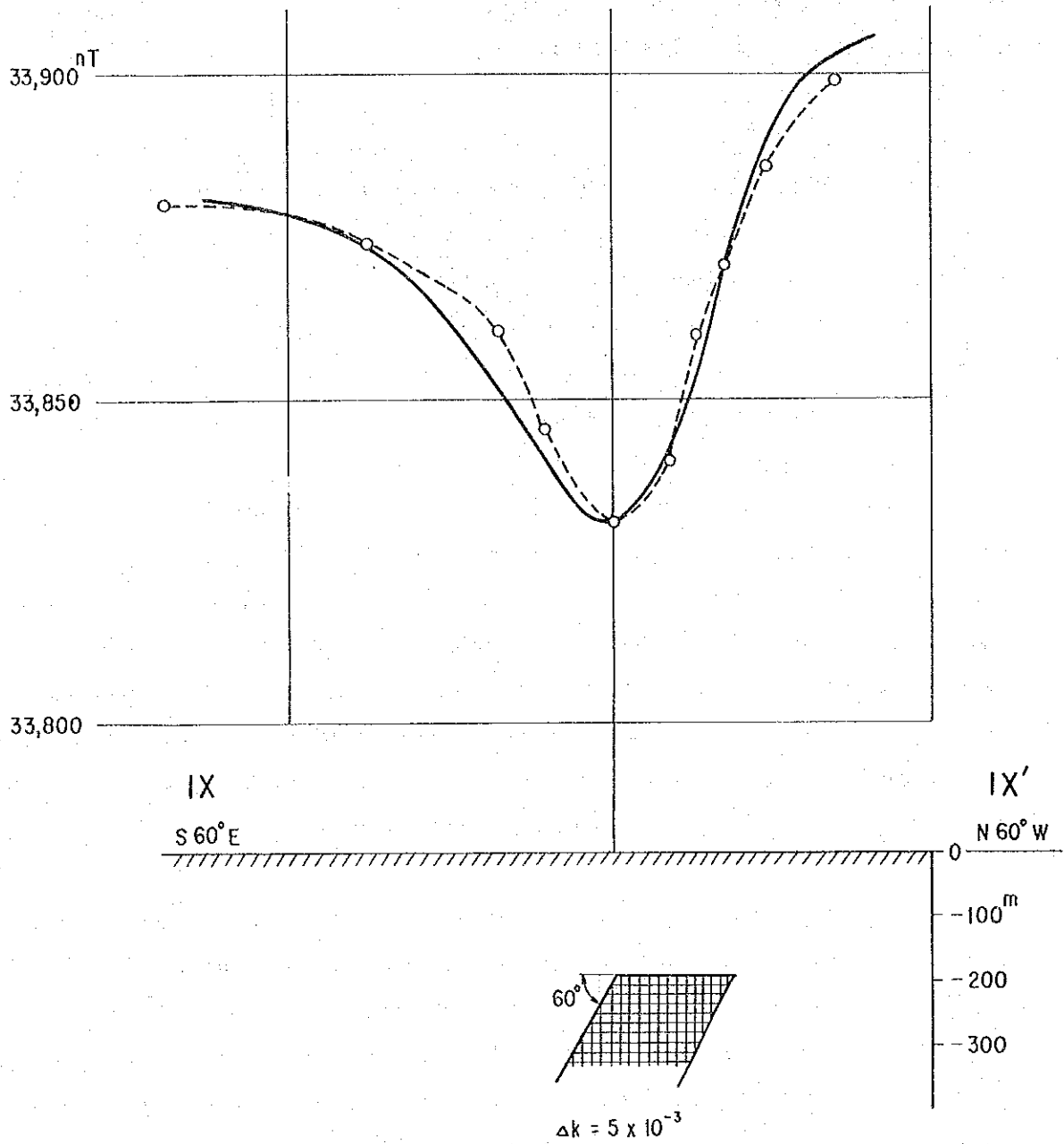
Fig. 2-12(9) Principal Profile of the Magnetic Anomaly

ratio of the magnitude of the positive anomaly and negative anomaly varies with the shape and inclination of the magnetic rock mass (cf. Fig. 2–8).

Two series of magnetic rock masses were analyzed in the northern part of the survey area and another series in the southern part. According to it, the mass on the eastern side in the northern part is 100 to 500 meters wide and about six kilometers long with the trend of N50°E to N20°E, about two kilometers. Among these magnetic masses, the one on the eastern side dips towards northwest at a low angle (about ten degrees) and the one on the western side dips 20° to 30° towards southeast, the opposite side of the above. According to the aeromagnetic survey conducted prior to this survey, these two series of magnetic anomaly zones were caught as two large in advance of this survey, these two series of magnetic anomaly zones were caught as two large magnetic anomalies showing different forms.

The magnetic rock mass analyzed from the aeromagnetic anomalies is at the center put between the two series of magnetic anomalies as shown in Fig. 2–13. It seems that the magnetic rock mass analyzed from the aeromagnetic anomalies represents the part of the intrusive vent corresponding to the root of the magnetic rock at relatively deeper part and that the two series of magnetic anomalies analyzed from the ground magnetic prospecting would represent the thinly extended part of the periphery of the mass taking funnel-like form at a shallow part. The depth of the magnetic rock masses analyzed from the ground magnetic prospecting is 50 to 200 meters below the surface and that of the one analyzed from the aeromagnetic survey is deeper than 250 meters below the surface.

While the magnetic rock mass detected in the southern part of the survey area was analyzed as the mass 100 to 400 meters wide and more than four kilometers long extending N40°E to N10°W on the whole, it is inferred that it could be divided into three parts and that they were bordered by the fault-like structures which is discontinuous magnetically. All these masses dip westward, and those on the northern side and the southern side show a low angle of 10° to 20° and the one at the center takes a high angle of 60° to 90°. Aeromagnetic anomaly was also detected at the position corresponding to the magnetic anomalies in the southern part, and the magnetic rock mass analyzed from the aeromagnetic anomalies seems to correspond to the core which will be the root of intrusive rock, showing a depth deeper than 300 meters, and the one analyzed from the ground magnetic prospecting seems to correspond to the expanded part of an umbrella of the mass in the shallow part.

2–3–5 Compilation

(1) The average values of magnetic susceptibility of the rock samples distributed in the vicinity

of the survey area and collected in this survey are as follows:

121.3 ~ 321.1 x 10^{-6} cgs. emu in the basement rocks (Mozambique metamorphic rocks).

For intrusive rocks, 202.05 x 10^{-6} cgs. emu in granite and 197.1 x 10^{-6} cgs. emu in gabbro. These are small in value.

4532.6 x 10^{-6} cgs. emu in serpentinite, showing by far the great value.

435.5 x 10^{-6} cgs. emu in basalt lava. Although this is relatively large in value, it is small as compared with common basalt (an order of 10^{-3}) (Table 2–3).

Strong magnetic anomaly detected in the survey area seems to be caused by serpentinites, and part of strong susceptibility in basalt may have caused the anomaly.

(2) Altogether three magnetic anomalies including the two series in the northern part and a series in the southern part, were detected in the survey area. The anomaly on the eastern side in the northern part extends for six kilometers in the NNE to SSW trend and the one on the western side in the same locality for two kilometers in the NE to SW trend have been strongly detected.

On the other hand, the anomaly group in the southern part shows a small amplitude, leading to an assumption that the magnetic rock mass analyzed from the above is emplaced in the relatively deeper part or may have low susceptibility.

(3) The magnetic rock mass analyzed from the groups of magnetic anomalies can be termed as dykes several hundred meters wide and several kilometers long.

Those in the northern part are assumed to dip in a low angle facing each other and to converge into one single dyke in the deeper subsurface. On the other hand, those in the southern part are assumed to dip westwards and to be latent in the southwest of the survey area.

(4) The results of the aeromagnetic survey and those of the ground magnetic prospecting are in consistent with each other in a general way. However, the forms of magnetic rock masses analyzed from those anomalies are different from each other. In contrast, the anomalies of ground magnetic prospecting are strongly pronounced at the contact of the magnetic rocks in the zone of low latitude of the earth's magnetism in the survey area, it is considered that the aero-magnetic anomaly obtained from high altitude of measurement would strongly reflect the central part of the rock mass. And this is the reason why they are different from each other. From these fact, it is highly possible that the magnetic rock mass analyzed from aeromagnetic anomaly would show the central part of the intrusive rock with a high susceptibility and the position of the magnetic rock analyzed from ground prospecting would indicate the peripheral part of the intrusive rock.

LEGEND

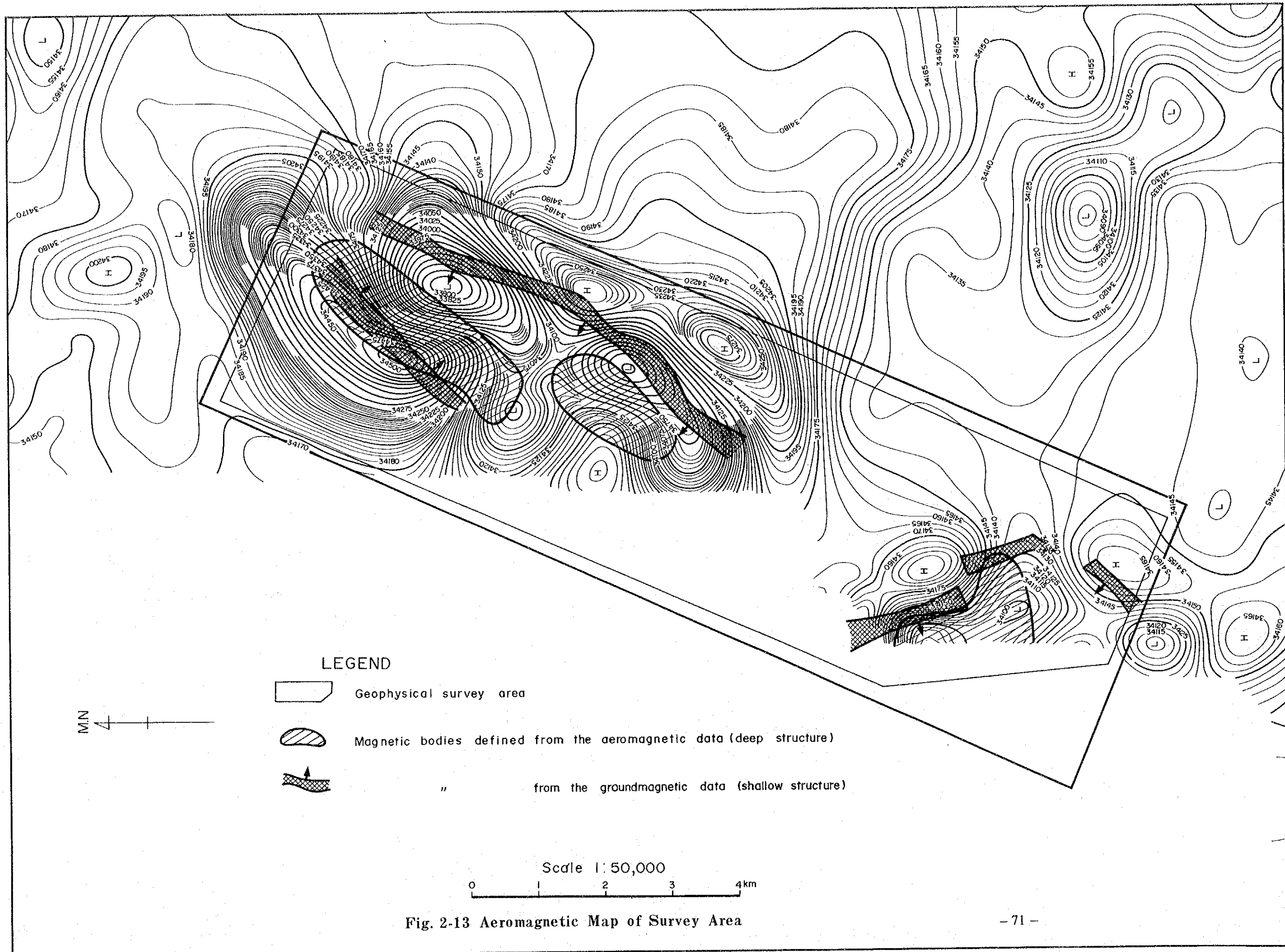▭ Geophysical survey area

⬭ Magnetic bodies defined from the aeromagnetic data (deep structure)

▰ " from the groundmagnetic data (shallow structure)

M.N

Scale 1: 50,000

0   1   2   3   4 km

Fig. 2-13 Aeromagnetic Map of Survey Area

— 71 —

CHAPTER 3 CONCLUSION

The following conclusions are reached based on the ground geophysical survey.

(1) Although the area belongs to the Mozambique Tectonic Zone, geology of the area is not clear because of extensive blanket sediments of Quaternary soil, river sand and gravel, and talus deposit overlying most part of the survey area. However, it is assumed that the basement is composed of regional metamorphic rocks classified as Mozambique metamorphic rocks intruded by dykes and stocks of granite, serpentinite and gabbro and that volcanic rocks including basalt extruded after Oligocene overlie the basement.

(2) The geologic structure of the survey area is basically composed of a syncline extending north-northwesterly and characterized by the presence of conspicuous overturned fold.

The faults of N-S to NNW-SSE, NE-SW and NW-SE systems are remarkable, and the whole project area is situated on the block bordering the western margin of the Rift Valley. However, the area in which geophysical prospecting was conducted lies within the Rift Valley separated from the block on the west by faults, and the geologic structure of NE-SW system seems to be widespread based on the rows and trend of the intrusive rocks and the distribution of gravity.

(3) The distribution of gravity in the survey area markedly reflects the geologic structure of the basement, and a steep inclination of gravity on the western side of the area reflects a faults structure dipping southeastwards.

On other hand, the central part of the survey area forms a low gravity zone, which leads to an assumption that the basement has been depressed in the central part of the area. The bottom of the depression reaches 250 meters below the surface while the difference of density between the basement rocks and the blanket sediments overlying the former is assumed to be 1.0 g/cm³.

(4) From the residual gravity anomaly, fault-like structure, presence of latent intrusive rocks, and a swell of basement are assumed in the basement structure.

(5) According to the test on physical properties of the rock samples collected in the survey area, the density of chromite ore is the highest showing an average value of 3.84 g/cm³ and those of the Mozambique metamorphic rocks of the basement is 2.57 to 3.07 g/cm³. In terms of intrusive rocks, gabbro shows 2.94 g/cm³ followed by 2.69 g/cm³ of serpentinite, and granite shows the lowest value of 2.52 g/cm³. Basalt shows 2.80 g/cm³.

As to magnetism of the rocks, serpentinite is 4,532.6 x 10⁻⁶ cgs. emu followed by basalt with a value of 435.5 x 10⁻⁶ cgs. emu, which was lower than the ordinary basalt. The basement rocks and other intrusive rocks show weak magnetism of 121.3 to 382.8 x 10⁻⁶ cgs. emu.

CHAPTER 3 CONCLUSION

The following conclusions are reached based on the ground geophysical survey.

(1) Although the area belongs to the Mozambique Tectonic Zone, geology of the area is not clear because of extensive blanket sediments of Quaternary soil, river sand and gravel, and talus deposit overlying most part of the survey area. However, it is assumed that the basement is composed of regional metamorphic rocks classified as Mozambique metamorphic rocks intruded by dykes and stocks of granite, serpentinite and gabbro and that volcanic rocks including basalt extruded after Oligocene overlie the basement.

(2) The geologic structure of the survey area is basically composed of a syncline extending north-northwesterly and characterized by the presence of conspicuous overturned fold.

The faults of N-S to NNW-SSE, NE-SW and NW-SE systems are remarkable, and the whole project area is situated on the block bordering the western margin of the Rift Valley. However, the area in which geophysical prospecting was conducted lies within the Rift Valley separated from the block on the west by faults, and the geologic structure of NE-SW system seems to be widespread based on the rows and trend of the intrusive rocks and the distribution of gravity.

(3) The distribution of gravity in the survey area markedly reflects the geologic structure of the basement, and a steep inclination of gravity on the western side of the area reflects a faults structure dipping southeastwards.

On other hand, the central part of the survey area forms a low gravity zone, which leads to an assumption that the basement has been depressed in the central part of the area. The bottom of the depression reaches 250 meters below the surface while the difference of density between the basement rocks and the blanket sediments overlying the former is assumed to be $1.0 \, g/cm^3$.

(4) From the residual gravity anomaly, fault-like structure, presence of latent intrusive rocks, and a swell of basement are assumed in the basement structure.

(5) According to the test on physical properties of the rock samples collected in the survey area, the density of chromite ore is the highest showing an average value of $3.84 \, g/cm^3$ and those of the Mozambique metamorphic rocks of the basement is 2.57 to $3.07 \, g/cm^3$. In terms of intrusive rocks, gabbro shows $2.94 \, g/cm^3$ followed by $2.69 \, g/cm^3$ of serpentinite, and granite shows the lowest value of $2.52 \, g/cm^3$. Basalt shows $2.80 \, g/cm^3$.

As to magnetism of the rocks, serpentinite is $4,532.6 \times 10^{-6}$ cgs. emu followed by basalt with a value of 435.5×10^{-6} cgs. emu, which was lower than the ordinary basalt. The basement rocks and other intrusive rocks show weak magnetism of 121.3 to 382.8×10^{-6} cgs. emu.

(6) Three large groups of magnetic anomalies were detected in the survey area, two series in the northern part and one in the southern part. Two intrusive rock masses are assumed to be present in the northern part and one mass in the southern part corresponding to the above respectively.

(7) It is considered that the center of a latent intrusive rock of high susceptibility is located at a depth deeper than 250 meters below the surface. It is highly possible that an intrusive rock with high susceptibility would most likely consist of ultrabasic rocks including serpentinite with a potentiality of chromite ore deposit.

Judging from the scale of latent rock mass, and the ore reserves and the ore grade of the known ore deposits distributed in the Telot serpentinite mass in the vicinity of the survey area, it appears impossible to expect an occurrence of a large-scale ore deposit. Moreover, the rock mass is found underneath the soft alluvial formation, and the Wei-Wei River with plenty water flows at the central part of the mass. Therefore it would be difficult to design as open pit mine from the topographical restriction and depth. Further, when taking the infrastructure into account, mine development might not be economically viable. Thus it does not warrant further exploration work.

However, in case exploration for the rock mass of high magnetism is carried out by drilling and other methods in future, it is recommended that the exploration work should be conducted for the rock mass of high magnetism in the northern part of the survey area, in order to select the target, where the depth of potential occurrence of intrusive rock is shallow.
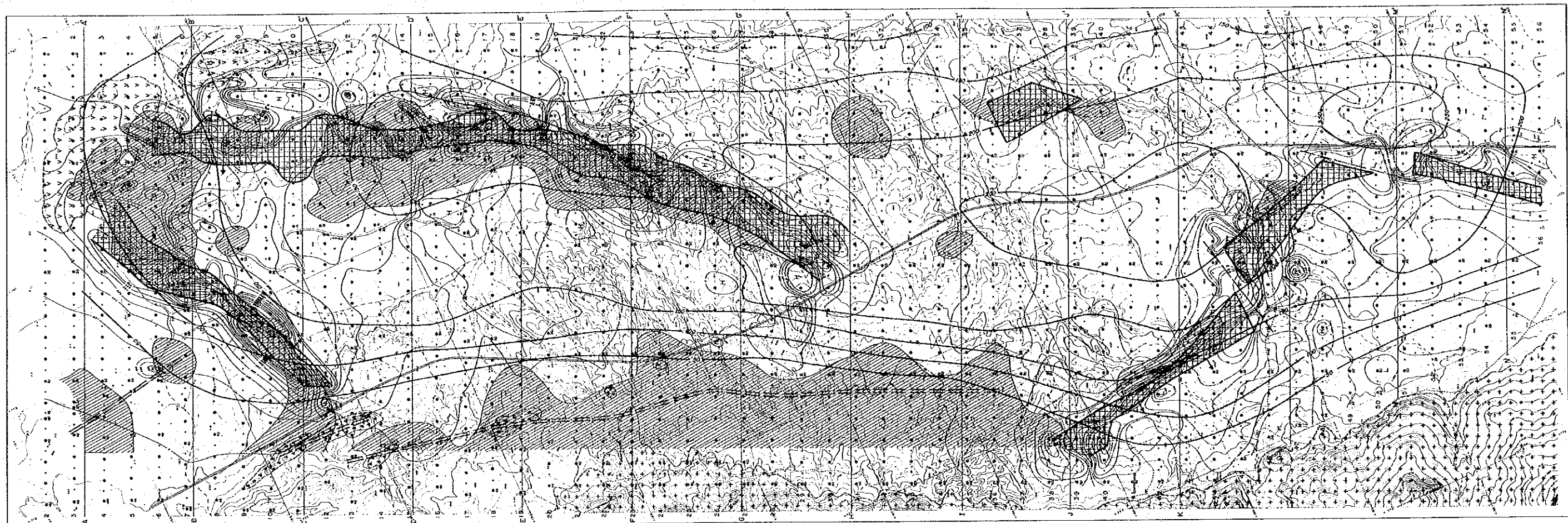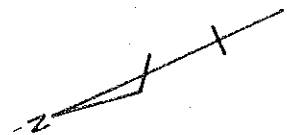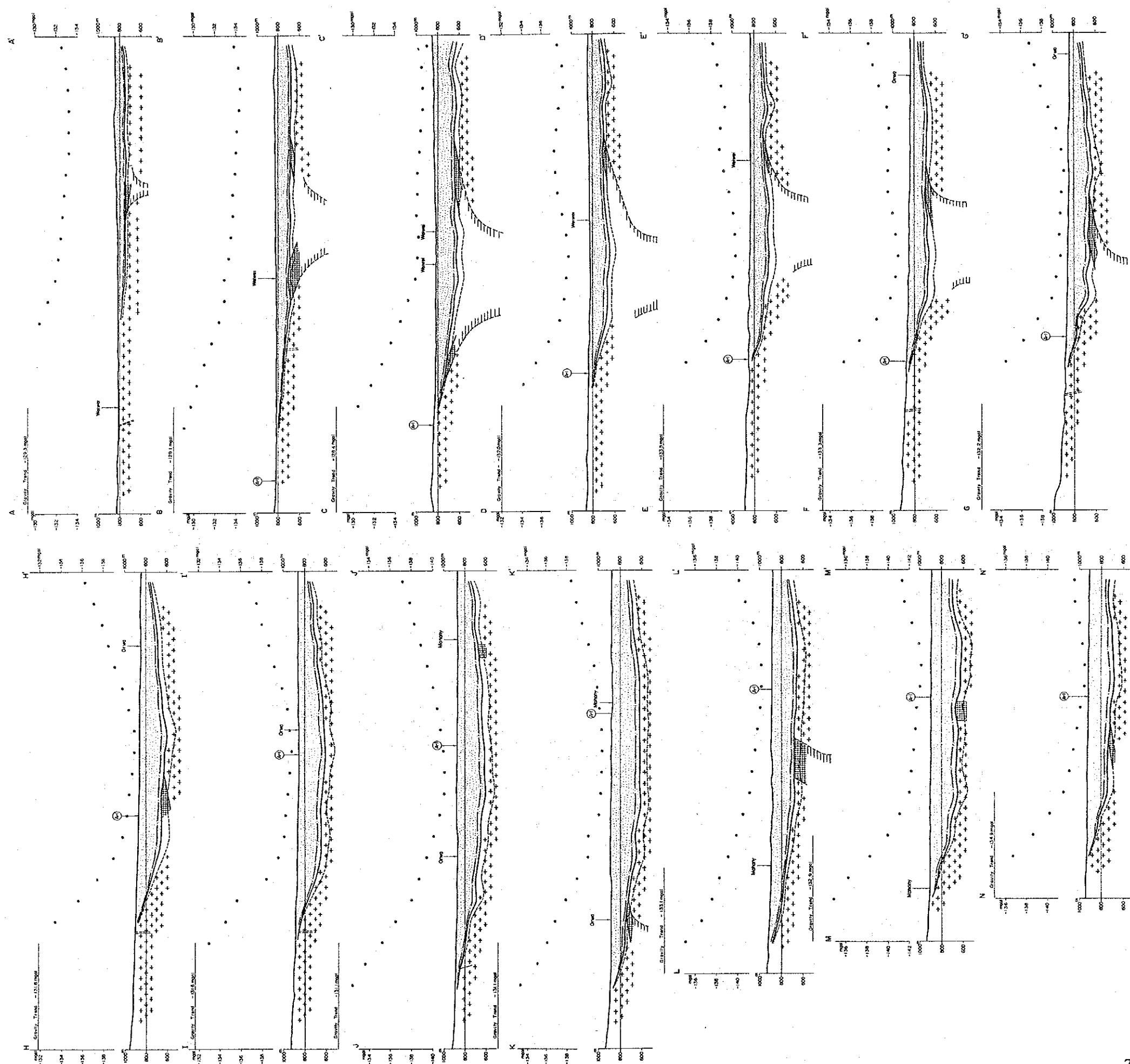
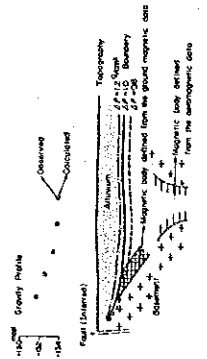Fig. 3-1 Interpretation Map

LEGEND

Fig. 3-2 Comprehensive Interpreted Magnetic and Gravity Cross-Section

REFERENCES

Grant, F.S. and West, G.F. (1965) : Interpretation Theory in Applied Geophysics, Part II
GRAVITY AND MAGNETIC METHODS, P. 235–254, P. 355–381.

Bhattacharyya, B.K. (1964) : Magnetic Anomalies due to Prismshaped Bodics With Arbitrary
Polarization, Geophysics, Vol. XXIX, P. 517–531.

Reford, M.S. (1964) : Magnetic Anomalies Over Thin Sheet, Geophysics, Vol. XXIX, P. 532–
536.

Talwani, M. and Worze, J.L. (1959) : Computations for Two-dimensional Bodies with Applic-
tion to the Mendocino Submarine Fracture Zome, Journal of Geophysical Research, Vol.
64, P. 49–59.

Spector, A. and Grant, F.S. (1970) : Statistical Models for Interpreting Aeromagentic Data,
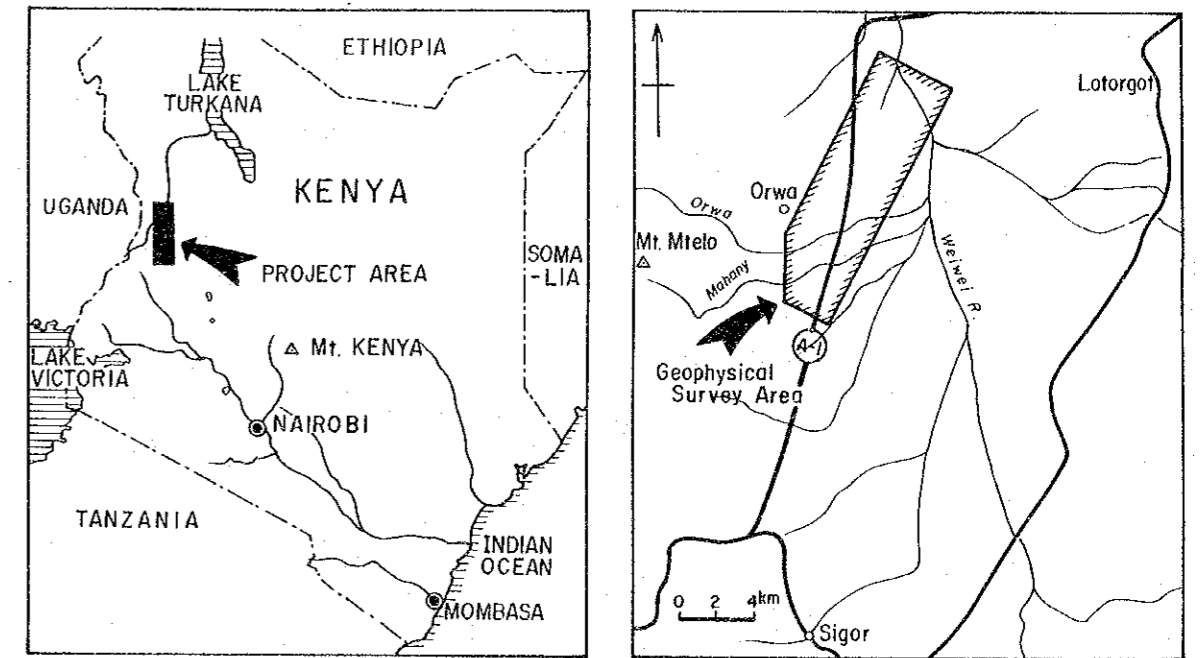Geophysics, Vol. 35, P. 293–302.

LOC
AN

UGANDA

LAKE
TURKANA

LAKE
VICTORIA

TANZANIA
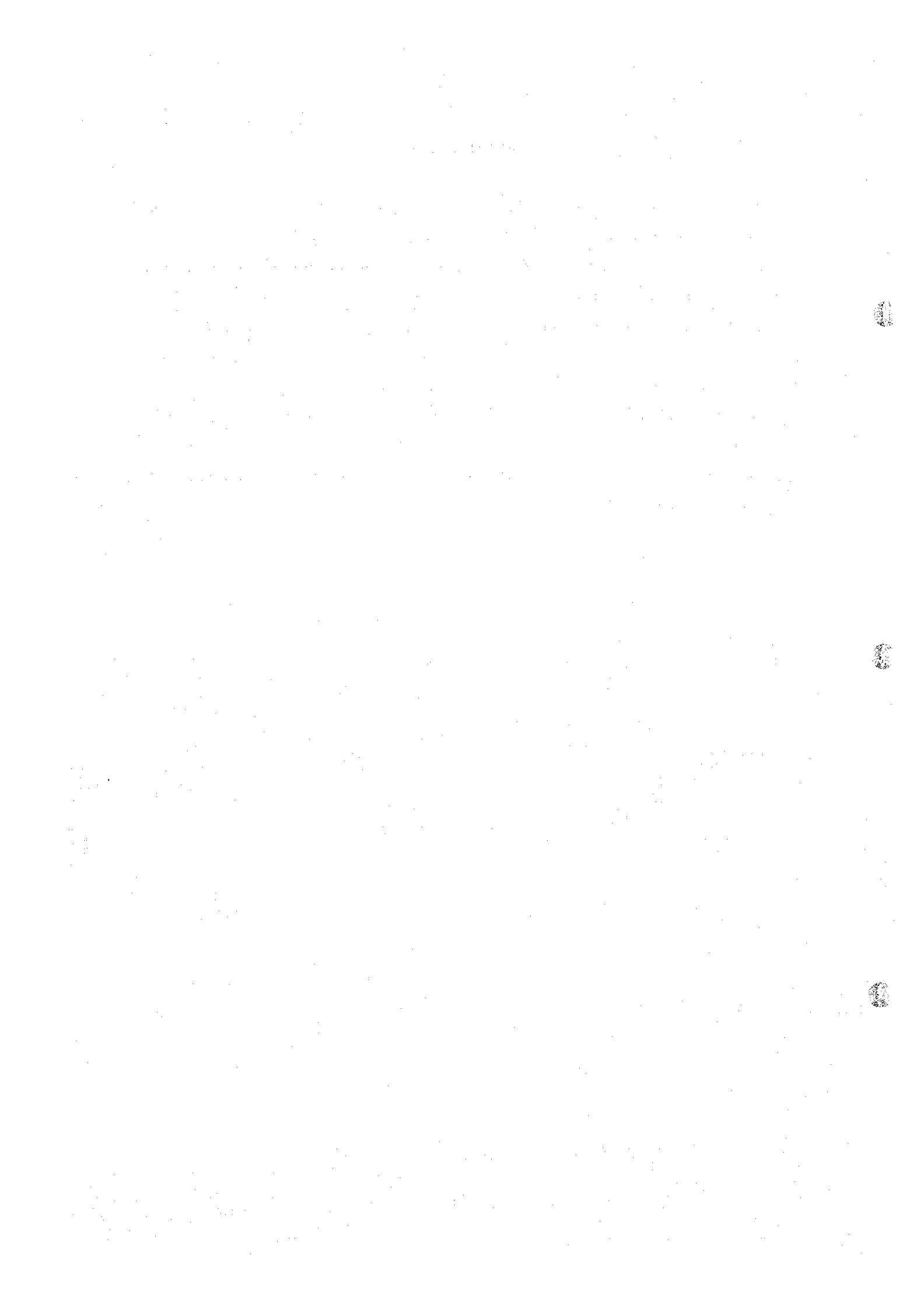
MINERAL EXPLORATION
IN
THE KERIO VALLEY DEVELOPMENT AUTHORITY AREA
(PHASE III)

LOCATION MAP OF MAGNETIC
AND GRAVITY SURVEY LINES

PL. I

LOCATION INDEX

JAPAN INTERNATIONAL COOPERATION AGENCY
METAL MINING AGENCY OF JAPAN
December 1985

Scale 1:10,000

0 100 200   500   1,000 m